BIOMEDICAL APPLICATIONS OF SPACECRAFT IMAGE PROCESSING TECHNIQUES--A PROGRESS REPORT

20 March 1967

JET PROPULSION LABORATORY

CALIFORNIA INSTITUTE OF TECHNOLOGY

PASADENA, CALIFORNIA

BIOMEDICAL APPLICATIONS OF SPACECRAFT IMAGE PROCESSING TECHNIQUES--A PROGRESS REPORT

20 March 1967

CONTENTS

ABSTRACT

During the past few years a considerable capability has been developed for computer processing of spacecraft-acquired image ("video") data. More recently, there has been increasing emphasis on the possible transfer of space technology to non-space applications. As a result, the Jet Propulsion Laboratory was encouraged to study the feasibility of applying these techniques to the processing of biomedical image data. This document is a progress report on the promising results obtained.

The established spacecraft image processing techniques are first discussed in some depth. Processed Ranger, Mariner and Surveyor pictures illustrate techniques such as geometric correction, photometric correction and enhancement, noise removal, and resolution enhancement.

The biomedical areas which have been briefly examined to date range from chest X-rays and retinal images to light microscopy image enhancement of chromosomes. In a closely related study, an optical tracking device has been applied to the problem of establishing blood flow velocity. Graphic examples of the application of the previously developed image processing techniques to these biomedical areas are presented.

Finally, a brief discussion of electron microscope resolution is presented. It is shown that similar computer manipulation of data in the visual frequency domain shows promise of extending the resolution down to atomic dimensions of 1 Angstrom.

SPACECRAFT VIDEO DATA HANDLING

INTRODUCTION

A considerable effort and expense has been required to obtain close-up television images of the Moon and Mars through spacecraft cameras. It has, therefore, been considered necessary to develop techniques for image reconstruction and manipulation in order to retrieve the maximum possible information from these pictures.

Over the past seven years a sizeable effort has gone into developing hardware and digital computer software which take video pictures and transform them to meet our needs. Techniques have been developed which remove certain classes of noise and which transform the picture to correct for geometric, photometric and frequency distortions. Once the pictures have been digitized and corrected, it becomes possible to extract useful information in either statistical or graphic form. Specifically, Ranger photographs of the lunar surface have been interpreted in such a way as to convert the image brightness to elevation and the elevation has been further analyzed to gather statistical properties on surface roughness. It will be shown later in the discussion of medical applications how almost every aspect of this development is meaningfully transferable to many problem areas in biomedical image analysis.

RECEIPT OF DATA

At the outset it is necessary to emphasize the need for improved performance in whatever recording media which have previously been considered sufficient. The techniques we have for handling data reach much deeper into whatever pictorial information exists and is seriously impeded by

unnecessary random noises and information losses which previously went unheeded. Specifically, let us look at the last frame of Camera A on Ranger VII (see figure 1). It is a very good photograph and contains a lot of information when examined as a whole. But let us examine just that segment of the frame in the region of spacecraft impact, which is at the lower right portion near the center (see figure 2). Under this magnification film grain appears to set the limit on resolution. When the picture is transmitted as a video signal, it is best to record it on magnetic tape rather than film in order not to restrict its dynamic range. The signal on tape was later digitized and played back under controlled laboratory conditions onto a high-precision film recorder to give the following picture (see Figure 3). Because the recording beam was more sharply focused (and therefore had a higher frequency response) more detail becomes visible. The most obvious new detail is the sudden appearance of a systemmatic pattern caused by a spurious oscillation on the spacecraft. It is just this kind of system limit which for future work must be carefully examined in order to utilize fully the total system recovery capability.

STRUCTURED NOISE REMOVAL

As an aid to interpretation, it is usually best to remove any image characteristics which are known to be spurious or non-contributing to the analysis. In some cases such corrections actually add false information, but this is known to the interpreter and there is no intent to deceive. For example, the reticle marking has been removed in Figure 3 by replacing the marking with the average of the information from both sides of the reticle mark. Similarly Figure 4 shows the removal of distracting streaks

Figure 1

Last frame of Camera A on Ranger VII made directly from analog recording.

Figure 2

Photographic blowup of segment of Figure 1. Film grain becomes visible.

Figure 3

Playback after digitizing on high-precision film recorder. (Reticle mark has been removed.) Increased resolution of recording beam spot brings out spacecraft system noise.

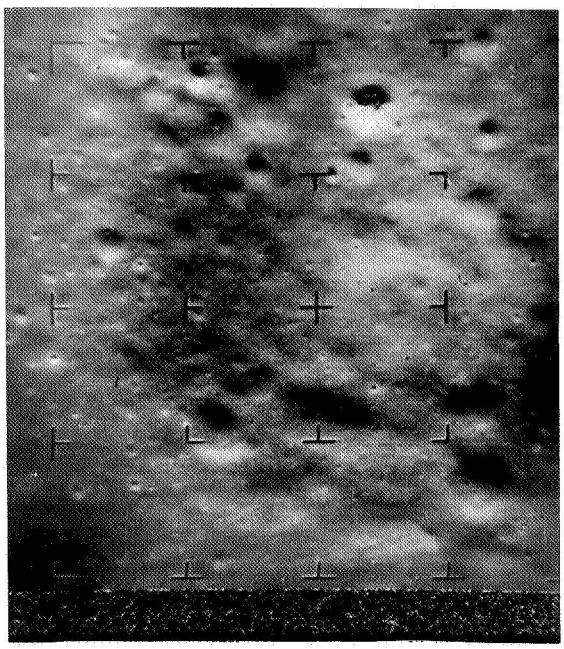

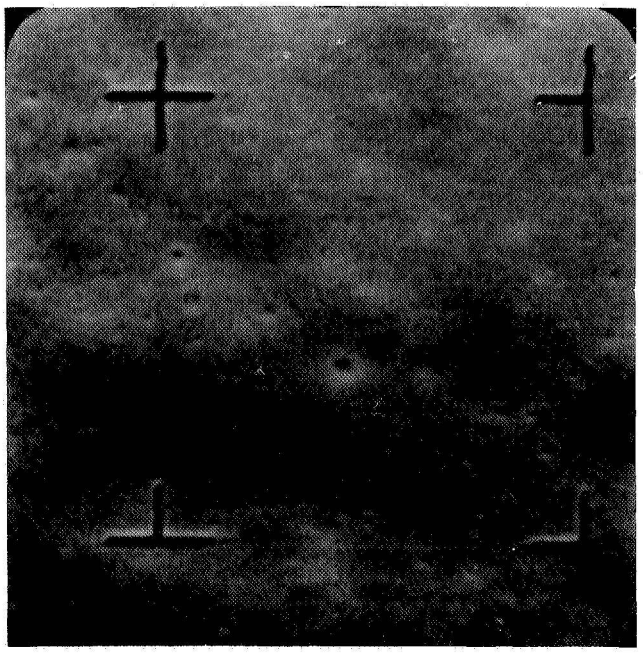

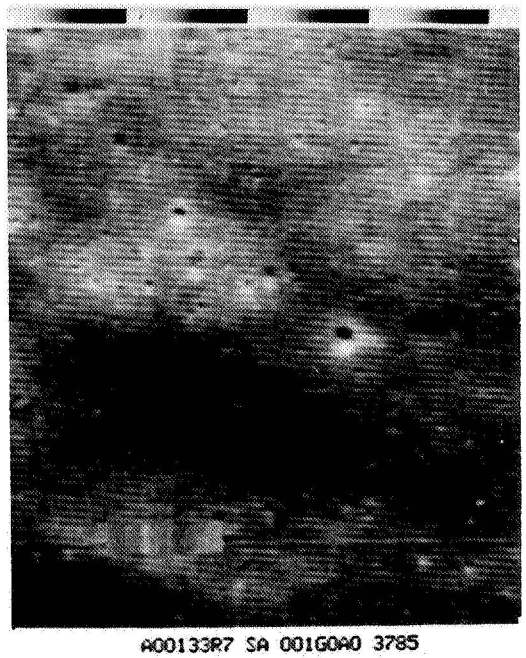

Figure 4

Mariner C, Frame 1

a. before streak removal

b. after clean-up and contrast stretch.

Figure 5

Ranger VII Final P1 Frame

a. before clean-up

b. after removal of spacecraft noise and subtraction of reticle.

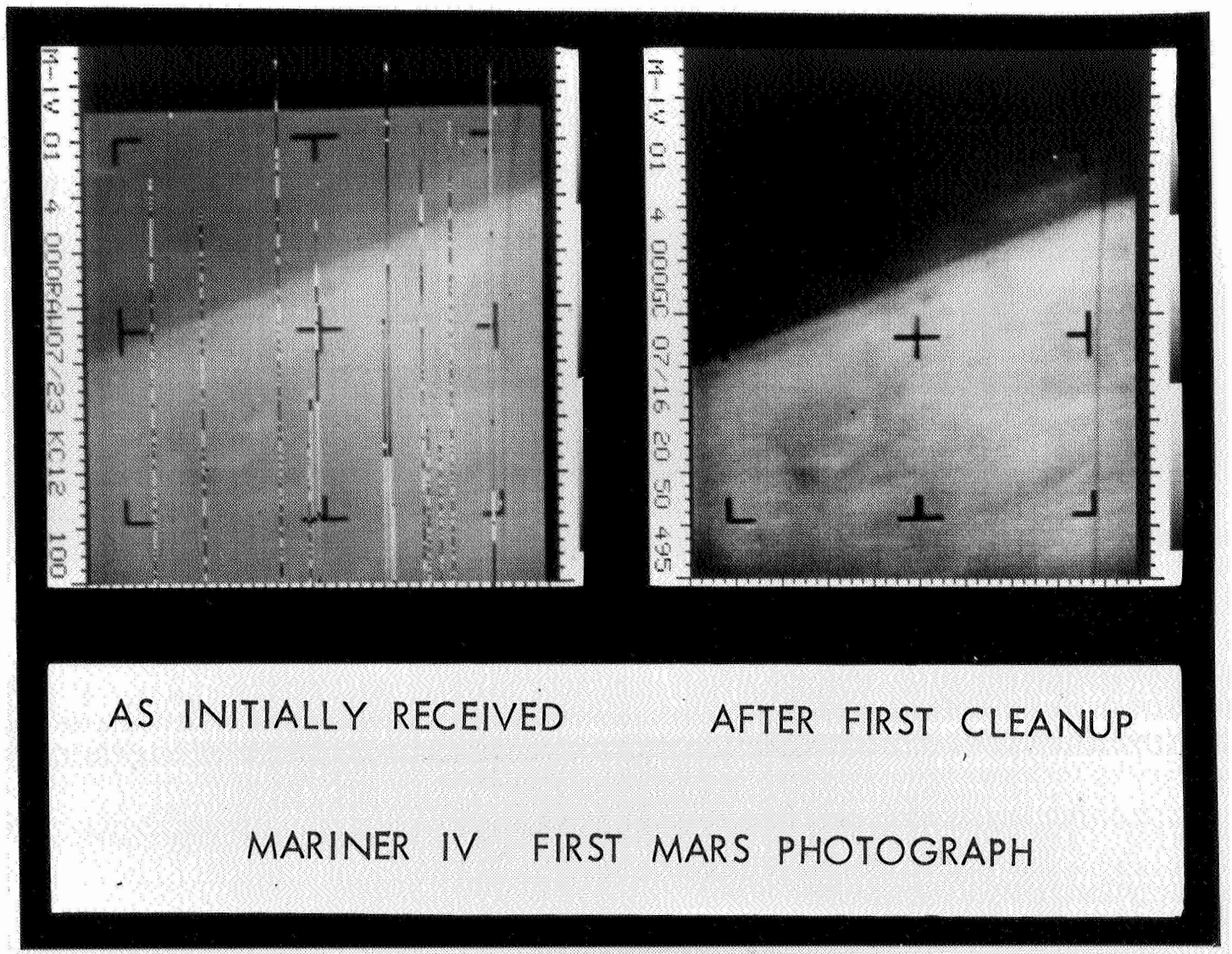

AS INITIALLY RECEIVED

AFTER FIRST CLEANUP

MARINER IV FIRST MARS PHOTOGRAPH

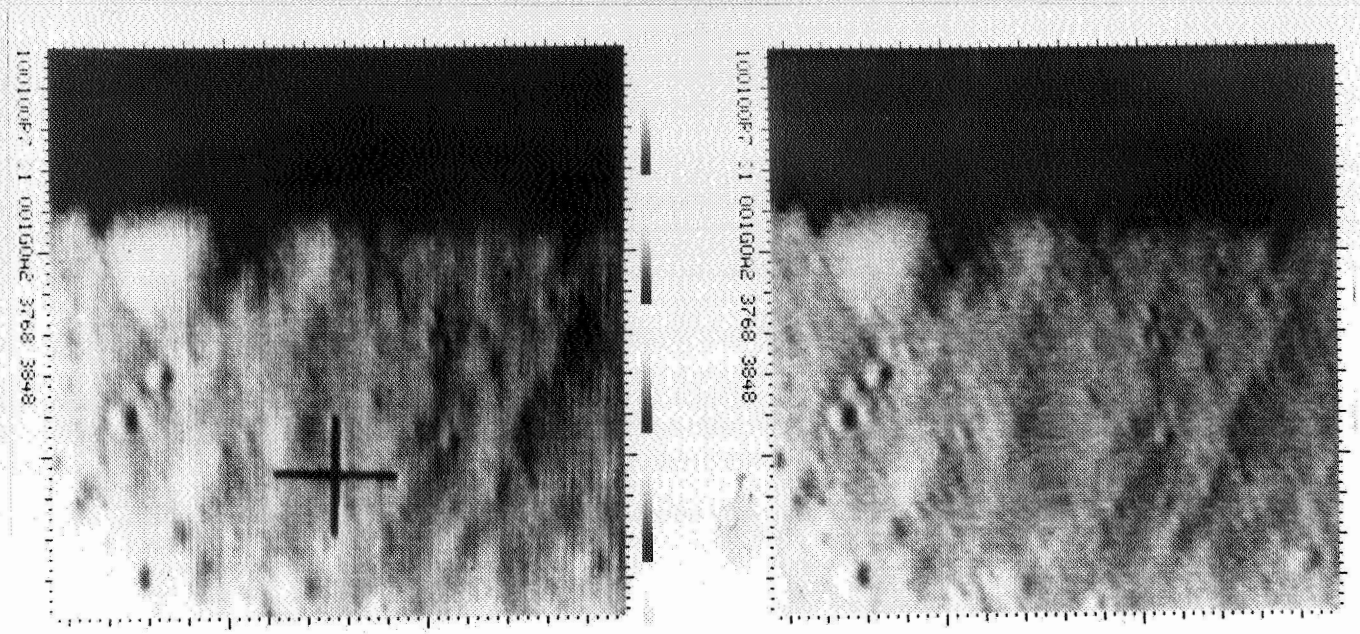

from Mariner IV frame 1 by replacement with neighbor averages.

Figure 5 (which comes from the Ranger VII P1 camera) illustrates removal of more complex noise distortions and required several operations involving removal of more than one frequency from the image each of which was assumed to be spurious. It is placed here to illustrate the kinds of noise removal possible. The process of manipulating (augmenting or removing) particular image frequencies will be discussed later.

PHOTOMETRIC CALIBRATION AND CORRECTION

Another type of system distortion is more evident in television cameras but does to some extent exist in almost all imaging systems. There is a non-uniform and also non-linear response to the input energy over the area of the sensor. In Figure 6, which shows frame 11 of Mariner IV, there is not only a lack of contrast but a "hot spot" near the upper left of the image caused by a non-linear photometric response of the vidicon camera.

(As long as we have frame 11, let us look at one experimental means of displaying the details of the image. Let us consider a typical numerical representation of the brightness of the points comprising the image to range from zero as white to 63 for black. Now if the contrast is stretched by a factor of eight, white would still be obtained for 0, but full black will have been reached by the time we got to 7. For the set of values from 8 to 15 let us represent them in brightness by going again from total white to total black. This process cycled a total of eight times is equivalent to ignoring the 3 most significant digits in a six bit number and displaying

Figure 9

Approximate high frequency enhancement of Figure 8.

Figure 7

Same as Figure 6, but display employs the three low order bits over full range giving "8-cycle" image. See text.

Figure 6

Mariner C, Frame 11--as seen from this orientation "hot-spot" appears in lower left.

Figure 8

Photometric calibration data applied to Figure 6 and contrast stretched.

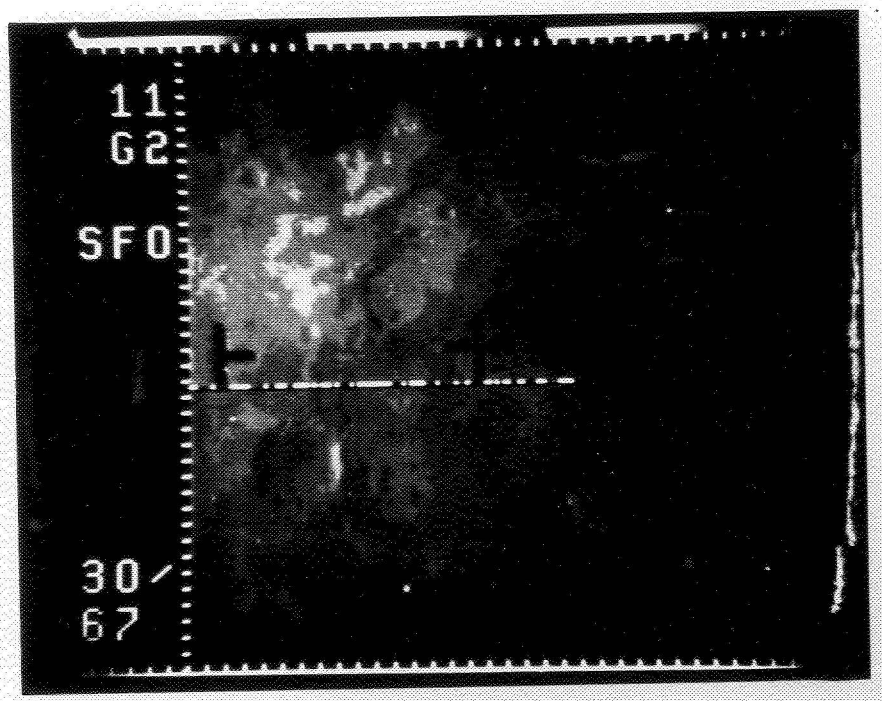
11
G2
SFO
30
67

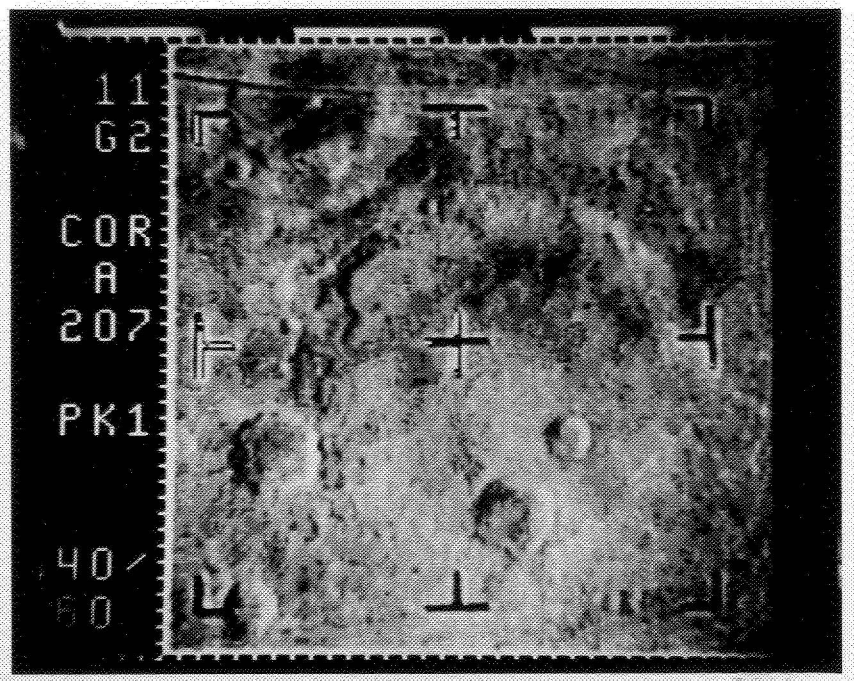
11
G2
COR
A
207
PK1
40
60

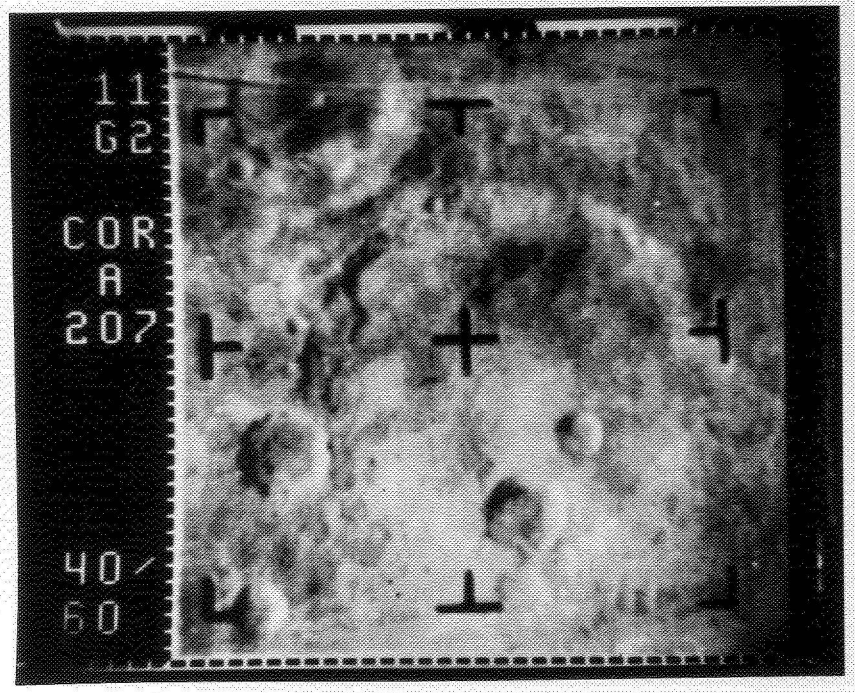
11
G2
COR
A
207
40
60

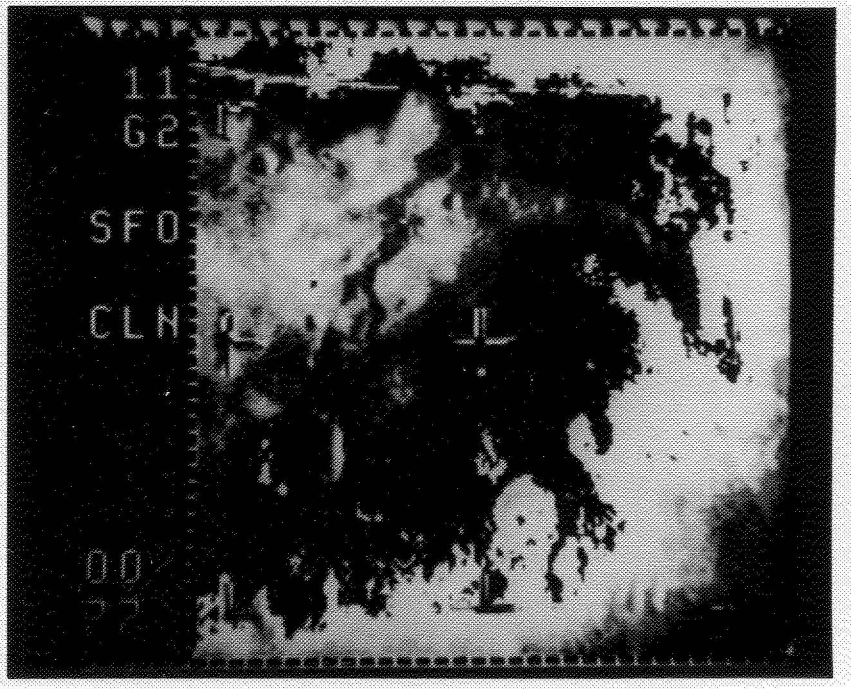
11
G2
SFO
CLN
00

only the least significant portion. But that is where the fine detail lies. This has been done in Figure 7. It is necessary when interpreting this kind of display to refer to the original for reference.)

If calibration data are collected which give the photometric response separately to black, gray and white for each point in the picture, a correction can be applied to the image to give absolute photometric response. An approximation to this is shown in Figure 8. The image now appears much flatter in intensity. (Again while we have Mariner IV frame 11 before us, Figure 9 shows an approximation to high frequency enhancement which will be described later.)

GEOMETRIC CORRECTION

The computer can take the values which represent brightness as an array of numbers in its memory and shift the position of these numbers around in a manner which changes their location in any image to be formed when these numbers are fed back out of the computer to make a new picture. An early Ranger camera had distorted the positions of a uniform square grid as seen in Figure 10. As the computer was being programmed to straighten this grid out, there was an "interim" product illustrated in Figure 11. This figure gives some feeling for the capability available for position manipulation. The desired corrected image was finally obtained and seen in Figure 12. This program was also used to reproject the image of the lunar surface as seen by the approaching Ranger camera to appear as though seen directly from above (See Figure 13). (And incidently, Figure 13b shows the same area as it has been interpreted into a 3-dimensional representation by converting the brightness of each point of the image to

Figure 12

Computer correction of geometric distortion seen in Figure 10.

Figure 11

Early computer attempt to straighten grid out.

Figure 10

Ranger III camera "sees" uniform square grid with geometric distortion

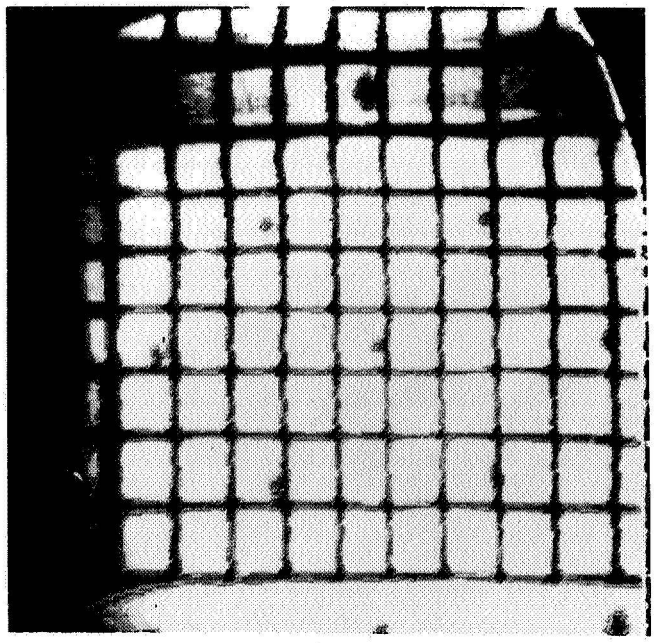

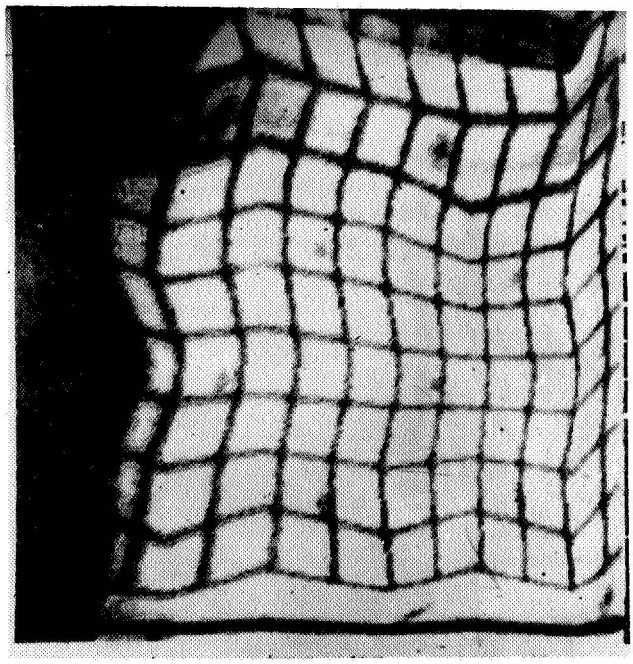

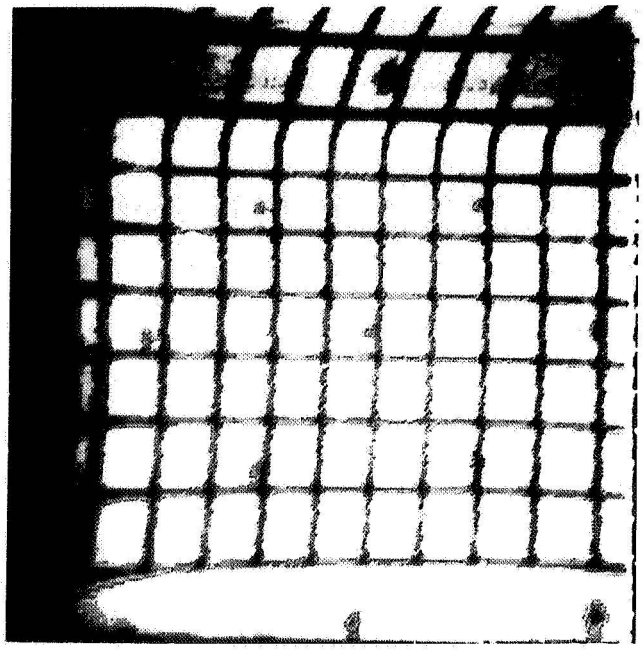

Figure 14

Ranger 8 camera P3 last frame illustrating direction of slope integration used to obtain elevations.

Figure 13

Ranger 8 camera, P3 reprojected normal to surface

a. normal intensity display

b. intensity converted to elevation with certain elevations saturated to black to give elevation contours.

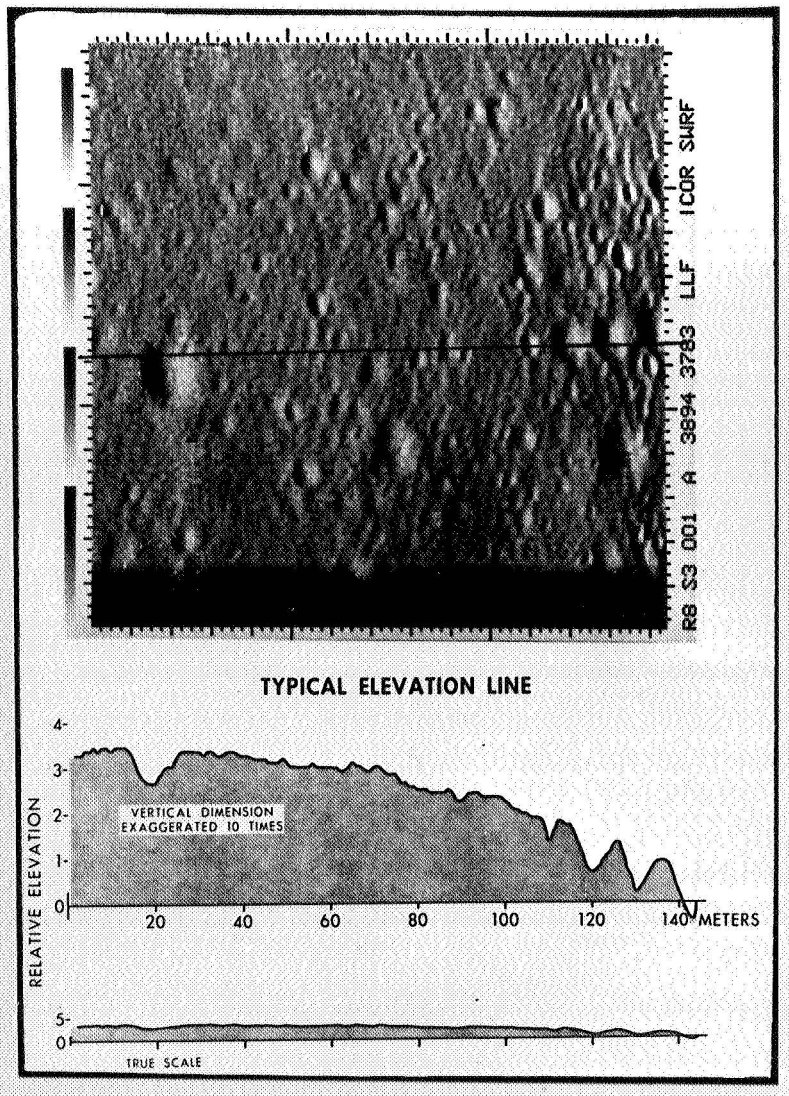
R8 S3 001 A 3894 3783 LLF ICOR SURF
TYPICAL ELEVATION LINE
RELATIVE ELEVATION
VERTICAL DIMENSION EXAGGERATED 10 TIMES
4
3
2
1
0
20
40
60
80
100
120
140 METERS
5
0
TRUE SCALE

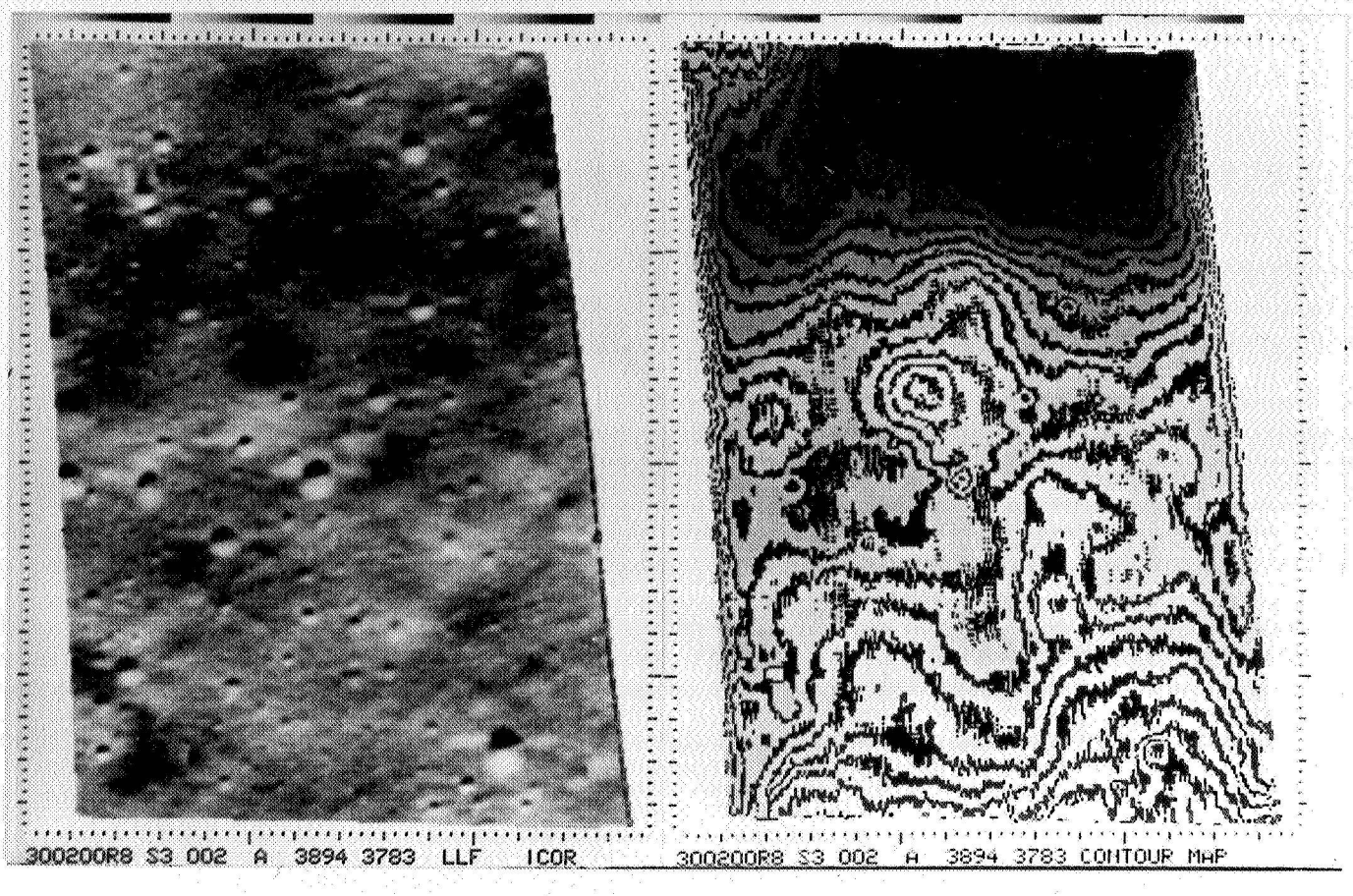
300200R8 S3 002 A 3894 3783 LLF ICOR
300200R8 S3 002 A 3894 3783 CONTOUR MAP

a slope and integrating the slope to an elevation. A particular profile is indicated in Figure 14.)

SINGLE FREQUENCY CORRECTION

Let us reexamine Figure 3 which is repeated here for comparison as Figure 15. There appears to be a distracting but regular pattern superimposed upon the desired image. (This image is made up from about 300 by 300 discrete digital elements.) Suppose we consider any particular region within this picture which is about 3 to 5 elements wide and about 15 elements high and compare it to a similarly sized array which consists of a wave moving in the vertical direction at about 5 picture lines per cycle. If the brightnesses (represented by numbers) of the corresponding pairs of points in each of the two arrays are multiplied together and all of these products are summed the result will be related to the degree of correspondence between the two patterns. Let this selected region of the picture be shifted in any direction and the process repeated until the whole picture has been covered. A new array of numbers will be created which represents the cross-correlation, or convolution, or filtering of the cosine pattern against the original picture. The result of this process appears in Figure 16 and represents the degree to which a narrow band of frequencies exist in the original picture. By applying an appropriate normalization factor and assuming that this entire pattern is unwanted, noise subtraction is performed and produces Figure 17.

HIGH FREQUENCY ENHANCEMENT

If it is possible to select some particular frequency from a picture and subtract it out, it should be possible to add or subtract a whole class of frequencies. Let us look at a picture in terms of its frequency

Figure 17

Subtraction of Figure 16 from Figure 15.

Figure 16

Map of noise calculated from Figure 15

Figure 15

Figure 3 repeated for comparison - Portion of Camera A Ranger VII

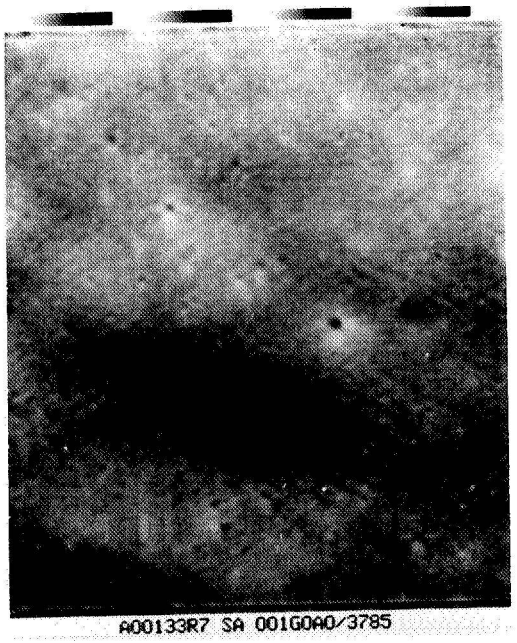

A00133R7 SA 001G0A0/3785

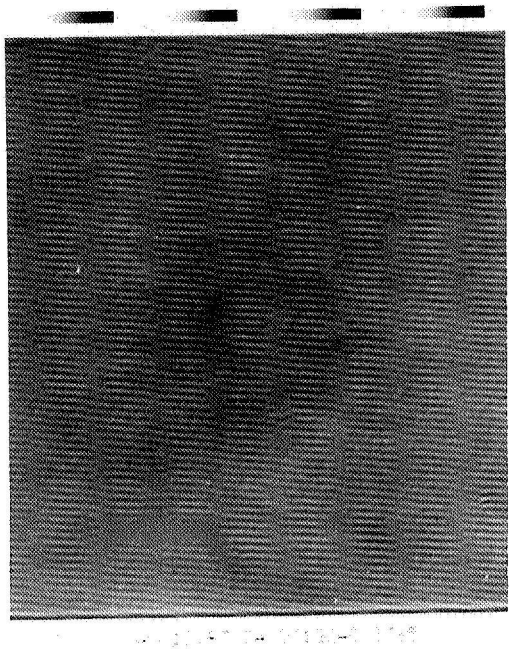

A00133R7 SA 001G0A0 3785

(Fourier) transform. In the frequency domain (using one-dimensional logic to begin with, the desired system response (modulation transfer function) would be unity for all frequencies out to the upper-limit cutoff (Figure 18a). Calibration measurements of the actual frequencies show the response illustrated in Figure 18b. If, for each frequency h the reciprocal of the response is plotted, then the curve plotted in Figure 18c results.

To avoid overemphasis of high-frequency noises, the upper bound of the curve is arbitrarily chosen not to exceed 5. The produce of the actual- and inverse-response curves (Figure 18d) gives a flat response out to the point where the original response has fallen to 1/5 its original value. The filtering program can again be applied, using the Fourier inverse of the reciprocal response. The convolution of this inverse function and the brightness of the original photograph enhances the higher frequencies to a point equivalent to the original scene. The effect of applying this correction can be somewhat startling and has the general effect of taking a picture and bringing it into sharper focus. In some respects this is literally correct since an out-of-focus image is equivalent to an attenuation of the higher frequencies. Three examples of high frequency enhancement are given in Figures 19 through 24.

Figure 18

One dimensional representation of frequency response of camera system. See text.

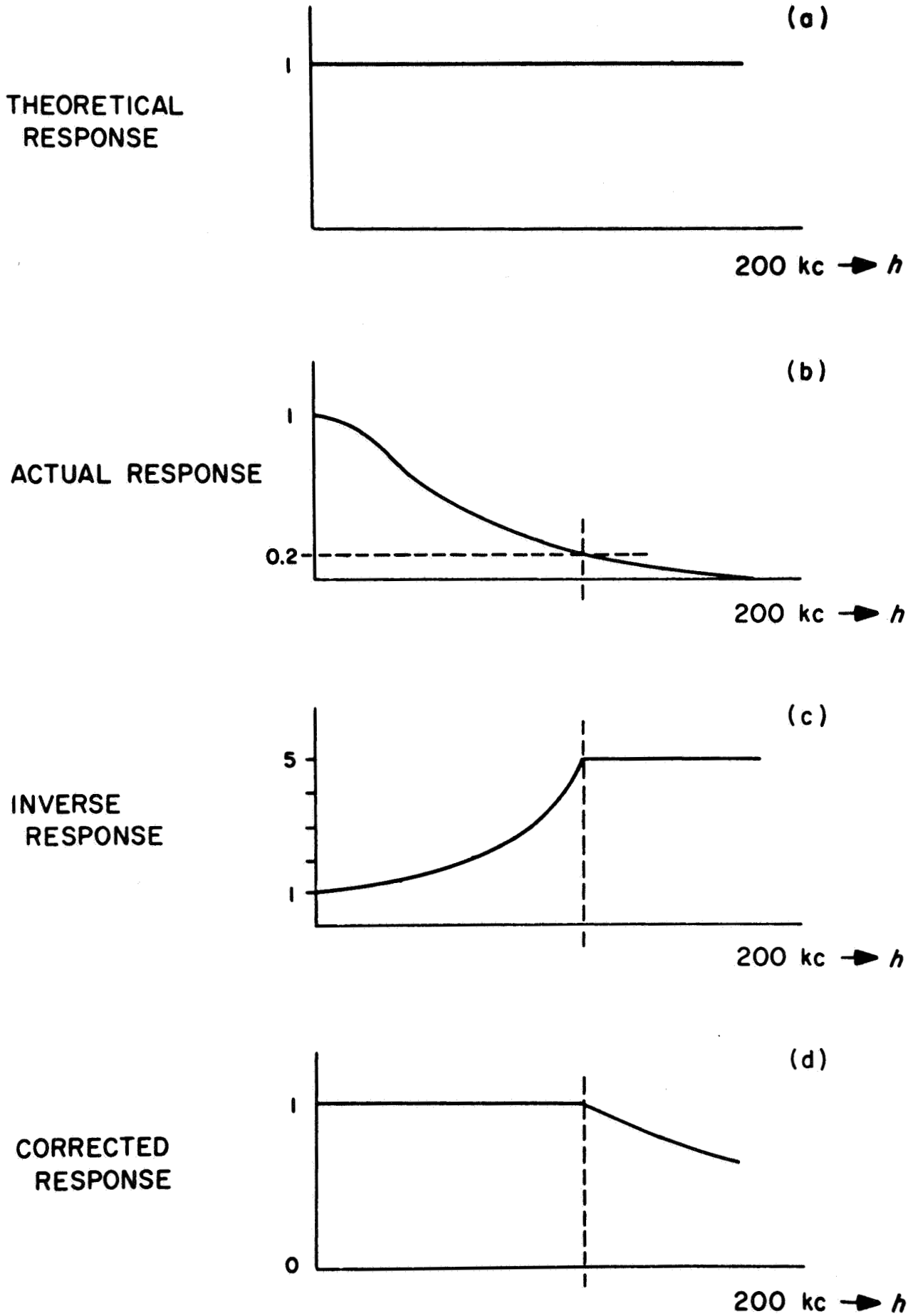
(a)
THEORETICAL RESPONSE
1
200 kc → h
(b)
ACTUAL RESPONSE
1
0.2
200 kc → h
(c)
INVERSE RESPONSE
5
1
200 kc → h
(d)
CORRECTED RESPONSE
1
0
200 kc → h

Figure 20

Figure 19 with corrected frequency response. Resolution target on spacecraft leg is now sharply defined. Ground texture is visible. Honeycomb material in footpad is in sharp relief.

Figure 19

Surveyor footpad

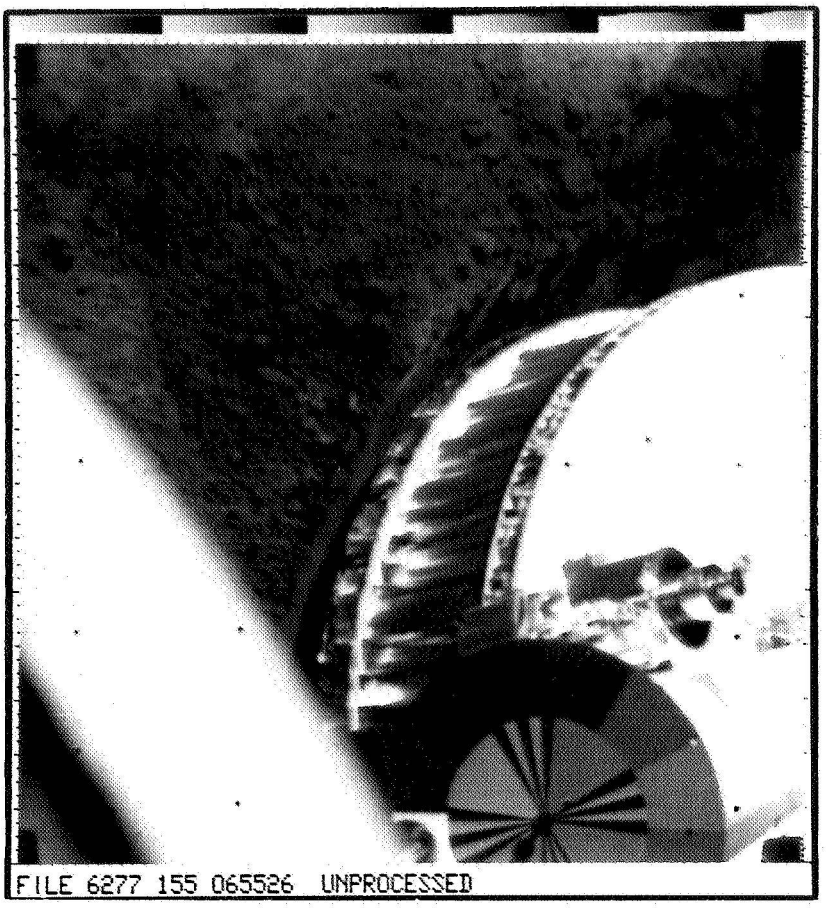
FILE 6277 155 065526 UNPROCESSED

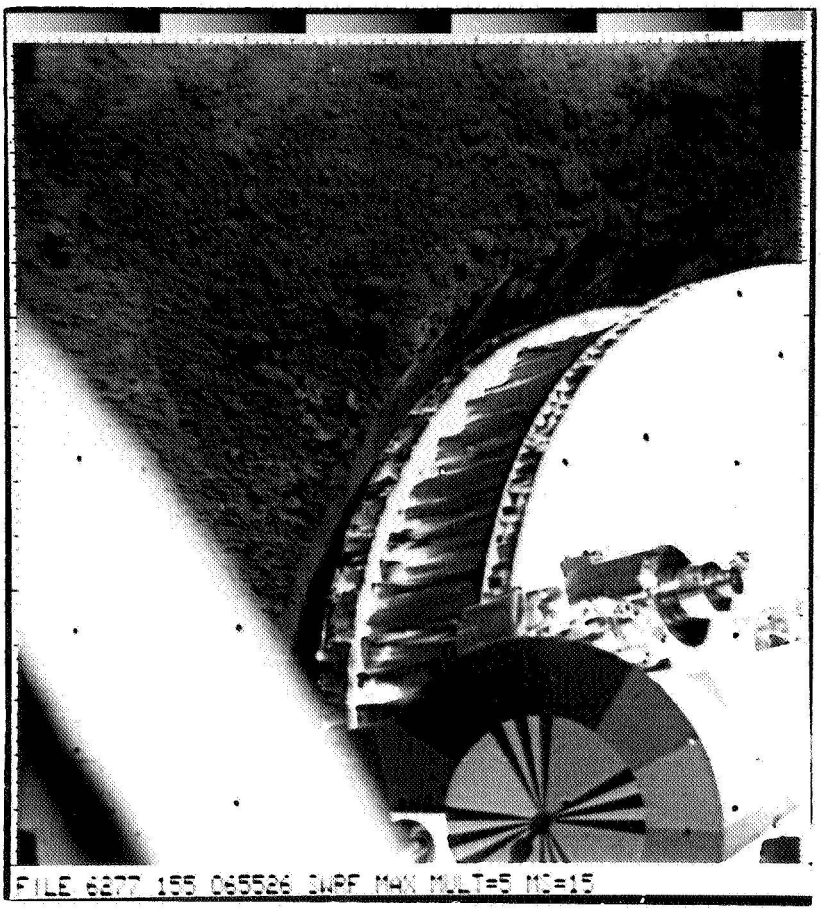
FILE 6277 155 065526 IWPF MAX MULT=5 MC=15

Figure 22

After high frequency enhancement

Figure 21

Lunar terrain as seen by Surveyor A camera

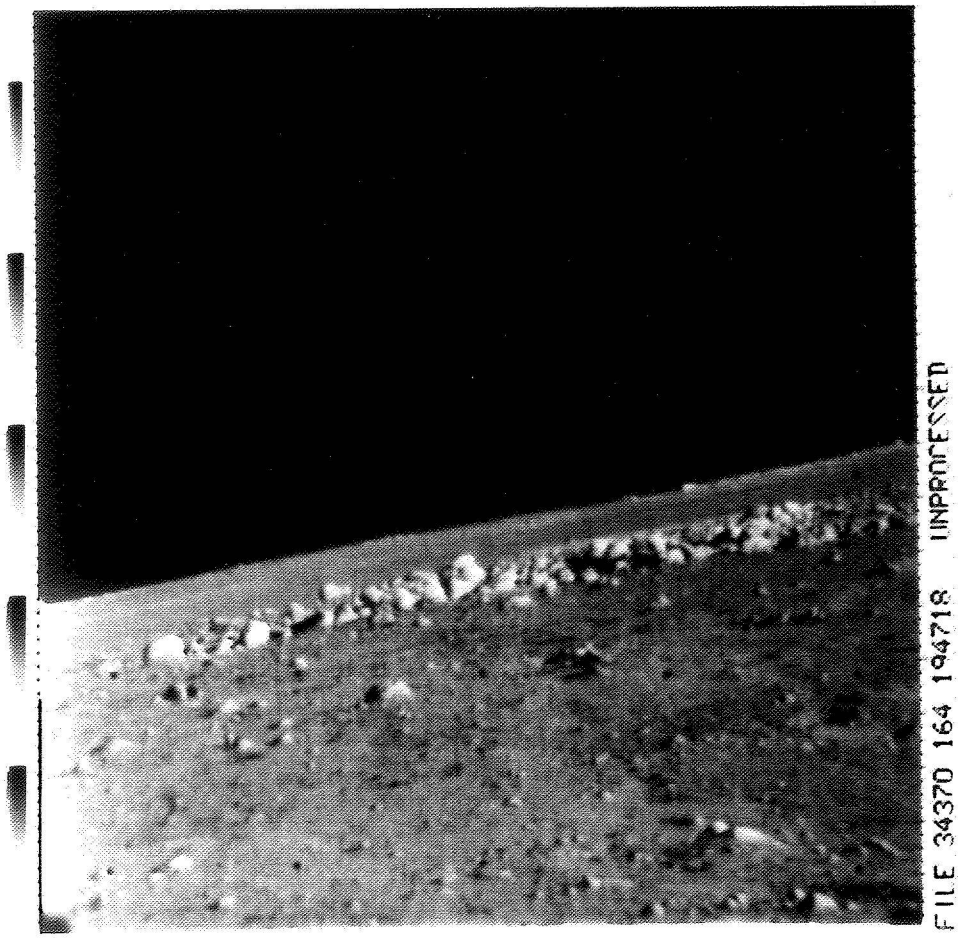

BEFORE ENHANCEMENT

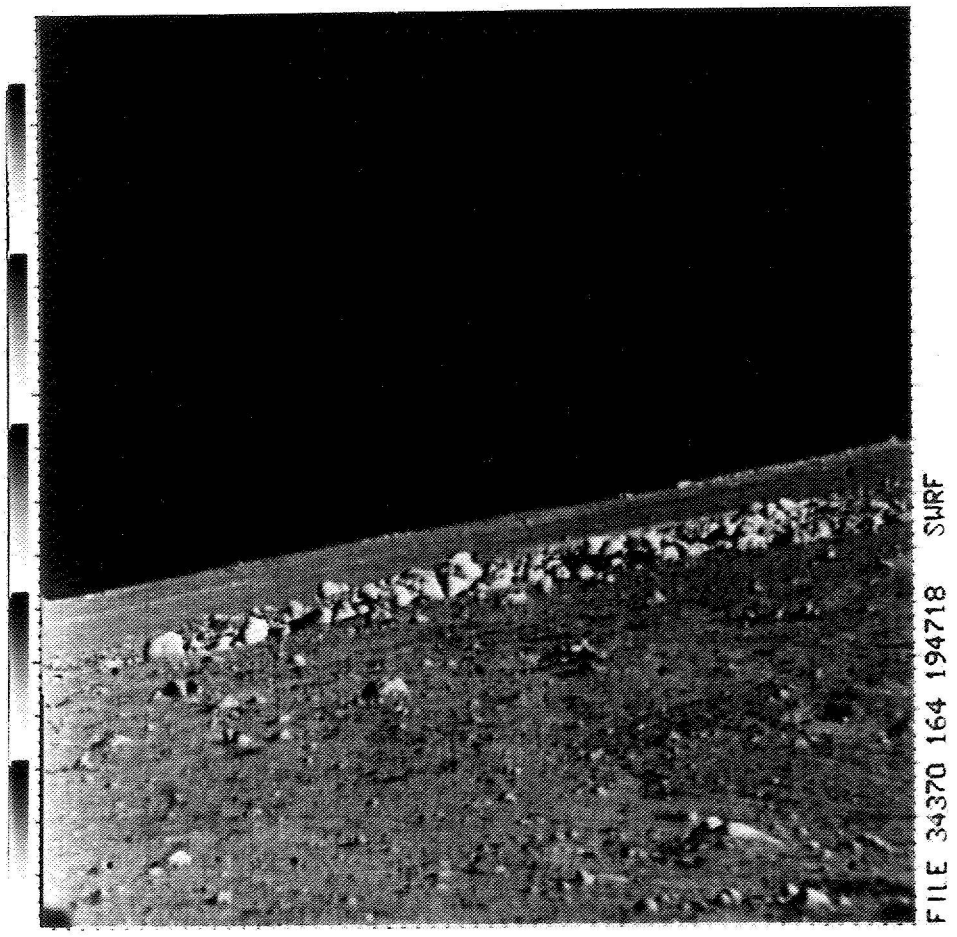

AFTER ENHANCEMENT

SURVEYOR MISSION A

LUNAR TERRAIN

Figure 24

Lunar "rock" enhanced

Figure 23

Lunar "rock" near Surveyor

ELITE 4300 12M 033301 ZMBE

ELITE 4300 12M 033301 MMBBDEZZED

BIOMEDICAL APPLICATIONS

During the past year, computer methods of image enhancement have been applied to a variety of biomedical pictures with the aim of evaluating their usefulness in the medical field. The initial results were quite encouraging, and of particular interest is the fact that when the early work was shown to a meeting of the American College of Radiologists last November in Chicago, the reaction was highly favorable. Part of their interest may stem from the fact that there is a severe shortage of radiologists in the United States so that technical assistance, either in the form of picture enhancement or ultimately in automatic pattern extraction methods, is quite welcome.

A number of examples are discussed below of the biomedical pictures processed during the past year. In addition, a description is given of several image processing problems which are of specific medical interest and are essentially solvable with the present technology, but which require more equipment or manpower than currently available.

SKULL X-RAYS

One of the first X-ray photographs processed was a skull X-ray in which a radio-opaque dye had been injected into the bloodstream in order to make the blood vessels visible. This technique is used both to study circulatory disorders and as a means of locating brain tumors that might cause artery displacement or constriction.

The unprocessed picture is shown in Figure 25. This picture was originally given to us by the UCLA Radiology Department as an 8" x 10" standard X-ray transparency. It was then photographically reduced to a

Figure 26

High frequencies restored from Figure 25.

Figure 27

High frequencies enhanced and low frequencies removed.

Figure 25

Unprocessed skull X-ray with radio-opaque dye injected into bloodstream

one inch square transparency in order to fit into our film scanner and finally scanned and converted into a 750 by 750 element digital picture. The unprocessed picture in Figure 25 was produced by reading the digital picture back onto film. There has been substantial picture degradation in this three-step process of reduction, scanning and playback, and the unprocessed picture in Figure 25 is considerably worse than the original 8" x 10" X-ray. It is hoped that these losses can be eliminated when the equipment becomes available which allows direct scanning of the original X-ray.

Figures 26 and 27 demonstrate two approaches to picture enhancement. The first, (Figure 26), uses digital filtering to restore high-frequency information lost in the fluorescent intensifying screens that are a standard part of most medical X-ray systems. The result of the filtering is to somewhat sharpen the image. The second approach, demonstrated in Figure 27, is to deliberately distort a picture in order to bring out a specific type of information. In this case, the information of interest was the blood vessels in the frontal portion of the skull and the processing involved application of an extreme filter that removed all low-frequencies (i.e., gradual shading changes).

Figure 28 is a skull X-ray in which air has been used to displace fluid in the ventricles of the brain. The air presents a better contrast media to the X-ray than the original fluid and allows inspection of the ventricle shape in order to detect possible brain tumors. An enhanced version is shown in Figure 29. The air injection is an extremely painful process, so it would be quite valuable to find a method to outline the ventricles without the air. Some preliminary efforts in this direction were not successful, but work is continuing.

Figure 28

Pneumogram before processing. The contrast medium is air pumped into the brain ventricles, which are normally fluid filled.

Figure 29

Enhanced pneumogram. The outlines of the ventricle are sharp, but some artifact has been created in the center.


EIGHT CYCLE CONTRAST OVERLAY

CHEST X-RAY FILMS--SUBTRACTION

Figures 30 through 36 demonstrate a quite different method--that of picture subtraction. Figures 30 and 31, provided by Dr. William Weiss, Director of the Philadelphia Pulmonary Neoplasm Research Project, shows chest X-ray films of the same person taken seven months apart, in which a lung cancer (shown by the arrow) is evident on the later film, but not on the earlier one. It was felt that subtracting the two pictures would remove unchanged data such as the ribs and thus emphasize differences such as that represented by the cancer. However, the pictures could not be directly subtracted because the rib positions were not identical on the two pictures. The rib positions were measured and the computer was used to force a match. The result of this part of the program, using the geometric distortion correction program developed for the Ranger TV cameras, is shown in Figure 32.

Figures 33 through 36 show the difference pictures after subtraction. Figure 33 is the picture resulting from subtracting the films without correcting the rib positions. The cancerous area is not evident. Figure 34 is the absolute difference picture after the rib correction and the lesion is now more evident. Comparison of the original in Figure 35 (which has gone through high frequency enhancement) and the strict subtraction in Figure 36 illustrates the effectiveness of removing low interest information.

RETINA PHOTOGRAPHS

Figure 37 shows a photograph of the retina in which a dye in the blood has again been used to illuminate the blood vessels. (Figure 38 is a blow up.) The light spot near the center is a tumor which could not be identified as being malignant or benign from the picture. Since the blood vessels

Figure 31

Chest X-ray taken September, 1954.
The cancer is indicated by the arrow.

Figure 32

The September film after application of a computer program to force the ribs to match the February film of Figure 30.

Figure 30

Chest X-ray taken February 1954. The cancer is not visible.

FY 2/54 UNPROCESSED

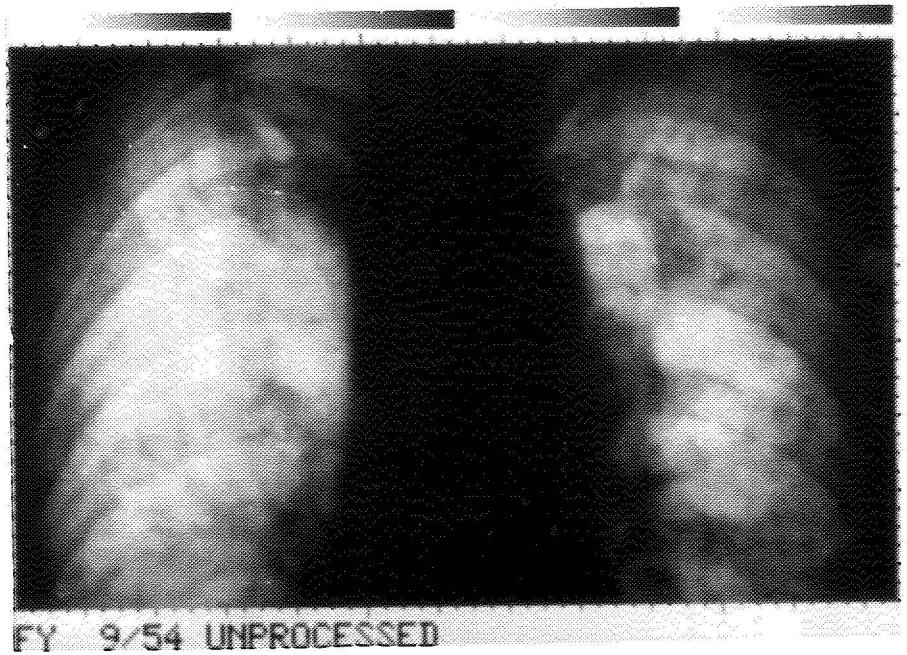

FY 9/54 UNPROCESSED

FY 9/54 AFTER GEOM

Figure 33

This is the result of an absolute subtraction of the two chest X-ray films without first correcting the rib mismatch. The cancer is only partially visible.

Figure 34

Absolute difference picture after rib matching was applied. The cancer becomes more evident.

Figure 35

September 1954 film after high frequency enhancement.

Figure 36

Result of strict subtraction of the early film from the later film. Negative differences were set to white.

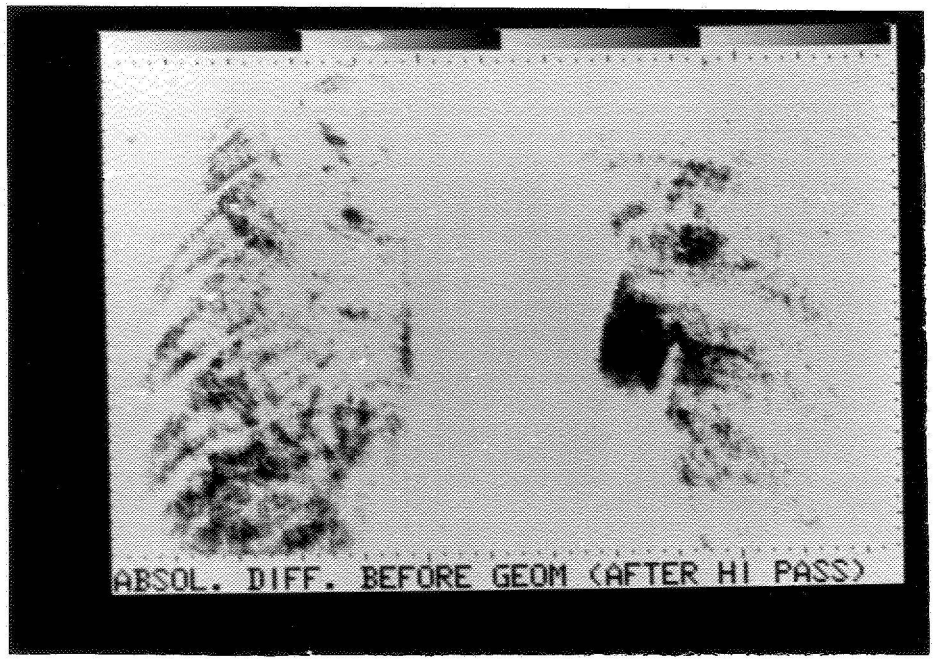
ABSOL. DIFF. BEFORE GEOM (AFTER HI PASS)

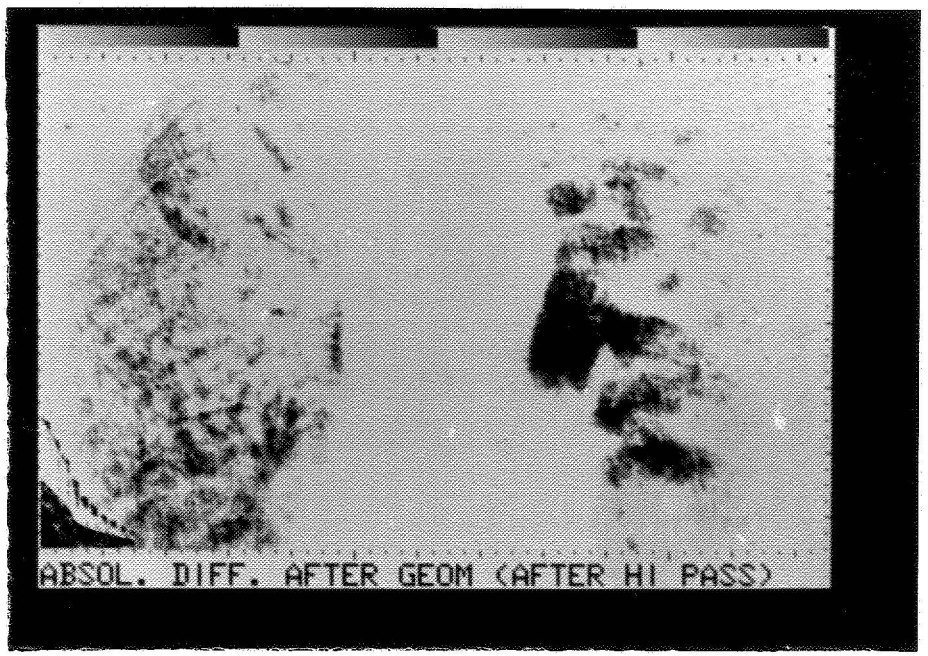
ABSOL. DIFF. AFTER GEOM (AFTER HI PASS)

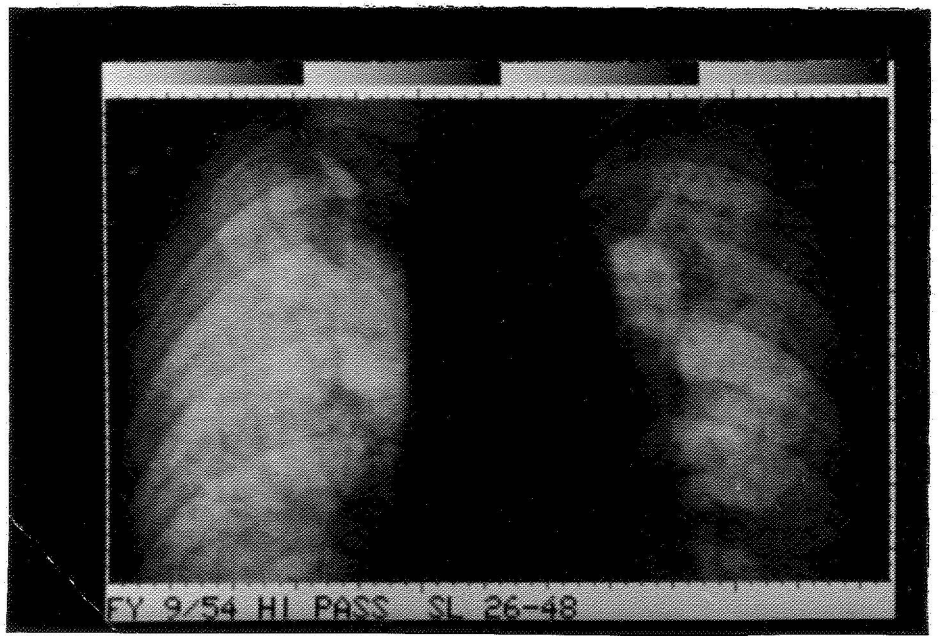
FY 9/54 HI PASS SL 26-48

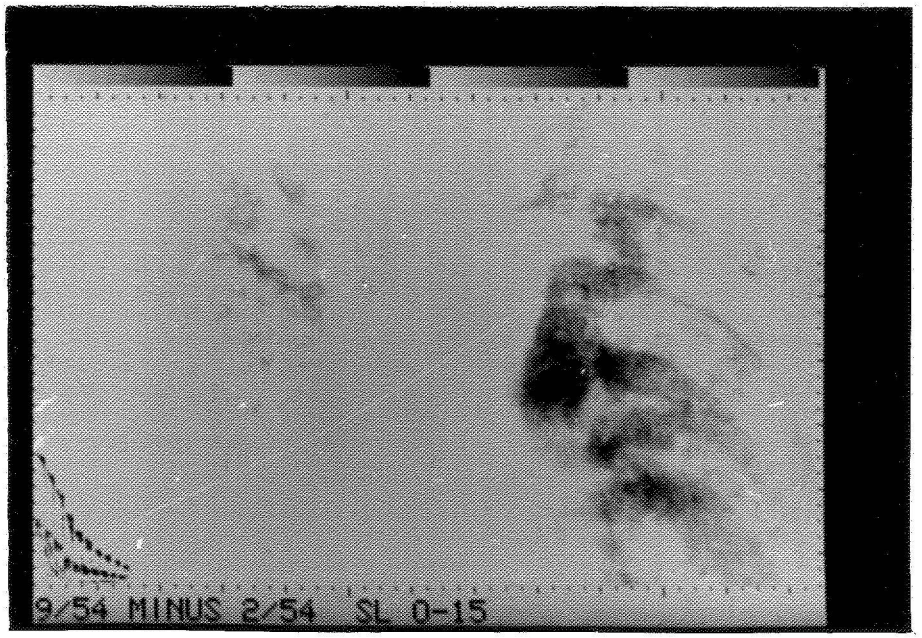
9/54 MINUS 2/54 SL 0-15

Figure 37

Photograph of the retina in which a luminescent dye has been injected into the bloodstream.

Fiture 38

Enlargement of the tumorous mass near the center of Figure 37.

Figure 39

Enhanced version of Figure 38.

Figure 40

Enhanced version of Figure 38

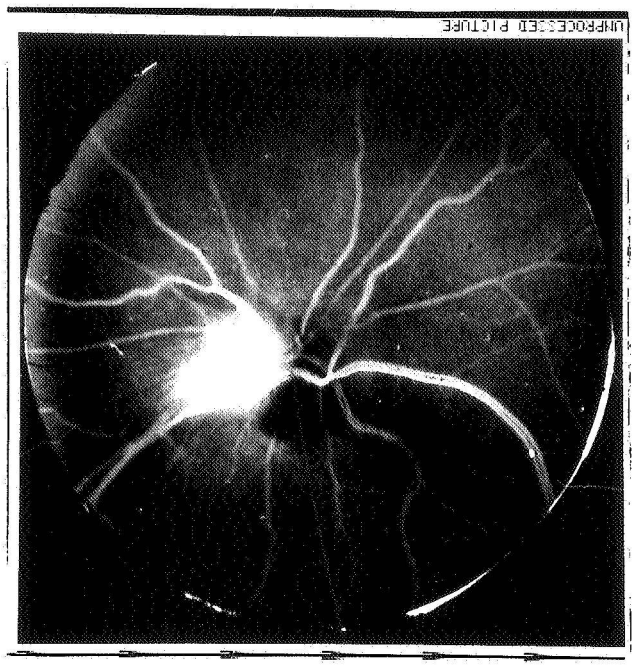

UNPROCESSED PICTURE

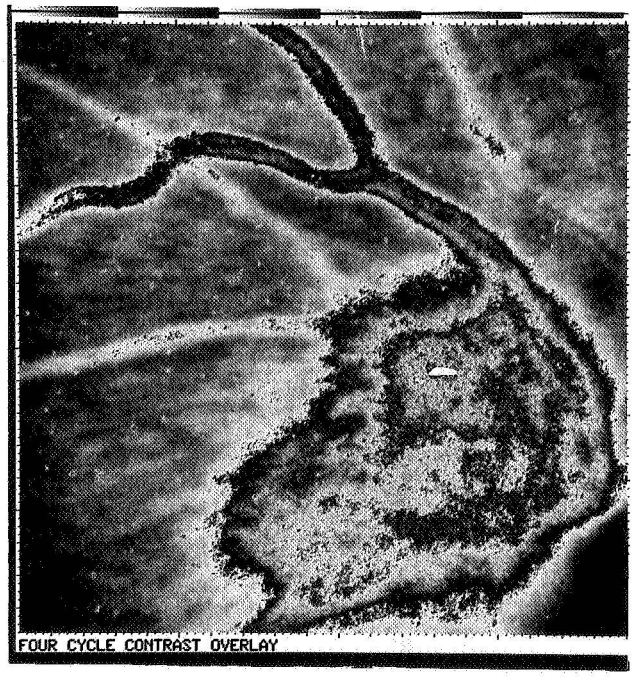

FOUR CYCLE CONTRAST OVERLAY

EIGHT CYCLE CONTRAST OVERLAY

sometime behave abnormally when passing through cancerous tissue, it seemed useful to enhance the arteries. Two rather preliminary efforts are shown in Figures 39 and 40. The results are inconclusive but interesting. Another reason to pursue work in this area is the fact that numerous diseases of the circulatory system such as arteriosclerosis, nephritis, diabetes and others are clearly reflected in the arteries of the eye. This, combined with the harmlessness of retinal photography make this a valuable diagnostic tool.

CHROMOSOME ANALYSIS

Another area suitable for computer processing is chromosome analysis--Figure 41 and 42 shows a chromosome at metaphase before and after filtering on the computer. This microscope picture was originally obtained by chemically inducing a white blood cell to undergo mitosis and then stopping the process just before the chromosomes split apart (i.e., at metaphase). It is at this instant that many congenital abnormalities in human beings can be identified by an abnormal chromosome count.

It is interesting that the analysis of chromosomes is a quite new field. It was not until 1956 that it was discovered that normal human cells contained 46 chromosomes instead of 48 as previously believed. In 1959 it was first noted that Down's Syncrome (mongolism) was associated with a chromosome count of 47. Since then, several other congenital defects have been found to be associated with whole chromosome abnormalities (presence or absence of an entire chromosome) and hundreds of partial chromosome abnormalities (missing or transposed arms, double arms, etc.) have been discovered, many of which are associated with specific genetic defects.

The usual method of chromosome analysis (called Karyotyping) involves sorting the chromosomes according to overall size and according to arm

Figure 42

High frequency enhancement of Figure 41.

Figure 41

Photograph of a microscope slide of a white blood cell chemically stopped at metaphase during mitosis.


METAPHASE CHROMOSOME

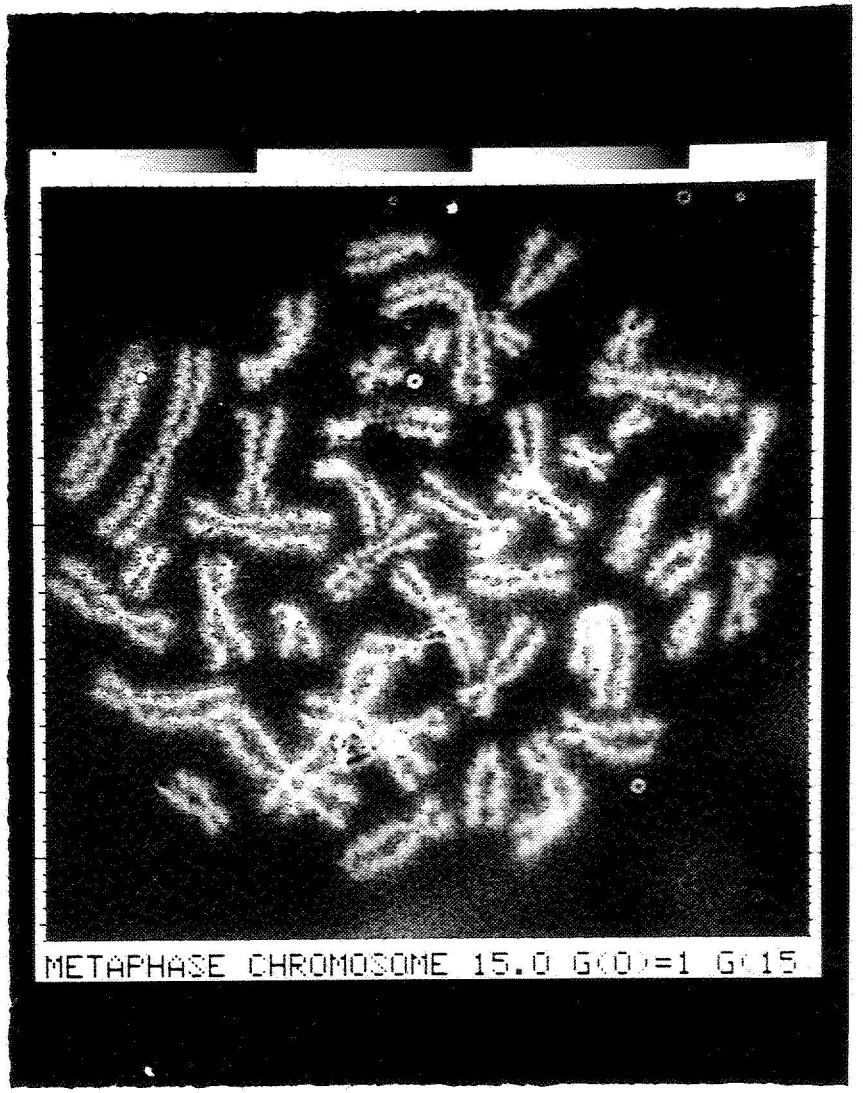
METAPHASE CHROMOSOME 15.0 G(0)=1 G(15

length. An example of a karyotyping chart where ten cells from the same individual were classified is shown in Figure 43. This is done with a pair of scissors and paste and typically one month is involved from the time the blood sample is drawn until the geneticist receives the chart.

There has been considerable work done in developing computer pattern recognition programs to do this sorting. The early programs simply counted chromosomes, looking for an extra or missing chromosome. More recently, programs are operating that look for the centromere and then calculate arm length ratios. However, these are essentially gross properties and there is reason to believe that abnormalities exist of a more subtle nature--that is, detail variation independent of arm length. As an example, Dr. John Melnyk, Chief of the Cytogenetics Department of Children's Hospital, who provided Figure 43 suggests that the number of helical turns in the arms may be an important feature to examine. This suggests computer enhancement now and study of the pattern recognition problem for possible future research.

Some additional enhancement methods applied to chromosomes are shown in Figures 44, 45 and 46.

MOTION PICTURE X-RAY FILMS OF THE HEART

There is considerable interest today in measuring heart volume and ventricular pressure as function of time. The reason for this is to be able to measure the amount of work the heart does, which in turn provides valuable information as to condition of the heart and the arteries. One method to make this measurement is to take high-speed X-ray motion pictures of the heart immediately after a radiopaque dye has been injected. The dye mixes with the blood and outlines the chamber. Each frame is inspected by hand and the volume calculated by hand. Pressure is recorded with a

Figure 43

Karyotyping chart, ten cells from the one individual are sorted according to overall size and arm ratio. From this chart, chromosome abnormalities are frequently identified.

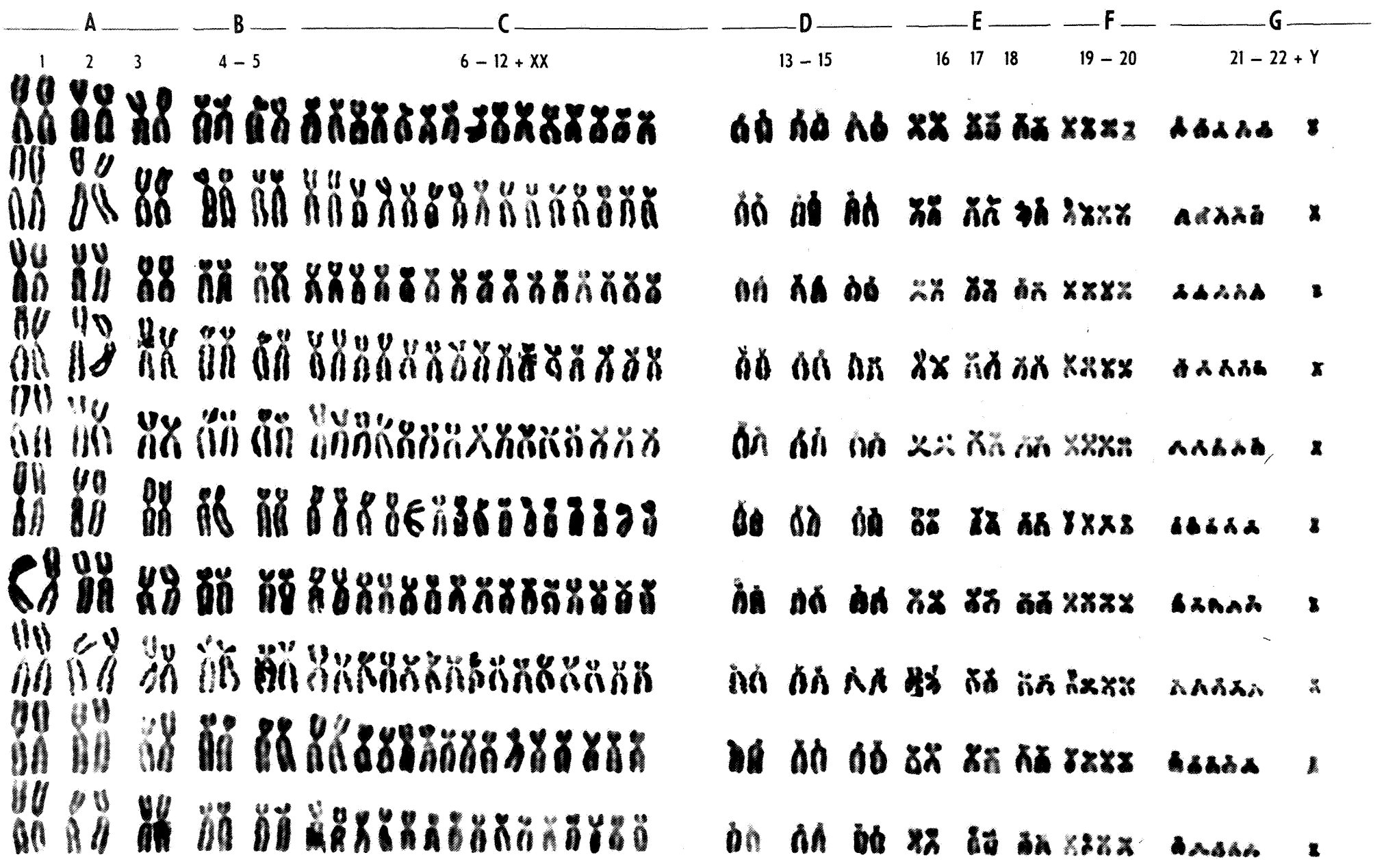

GOEBEL, J. ♂ 64-65 Partial 18 trisomy

Figure 44

Enlargement of a metaphase chromosome photograph

Figure 45 and 46 - Enhanced versions of Figure 44

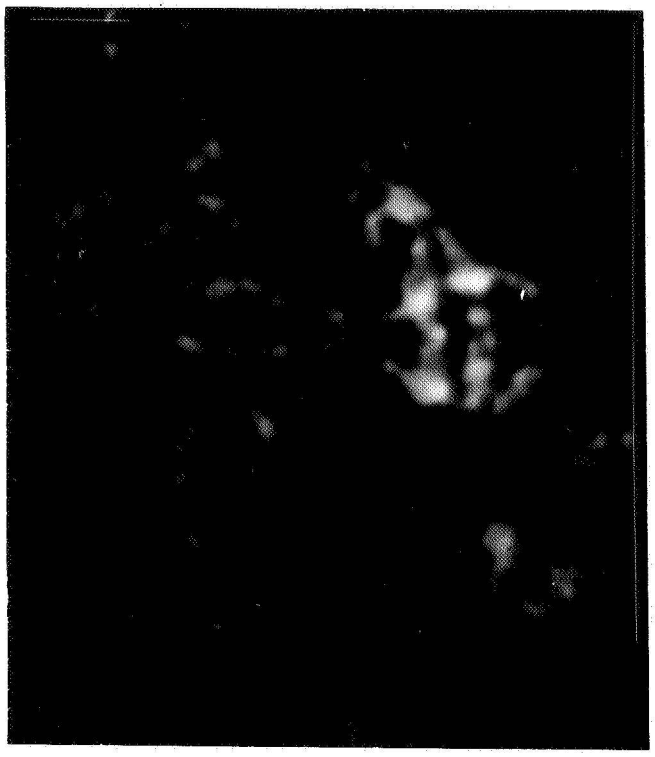

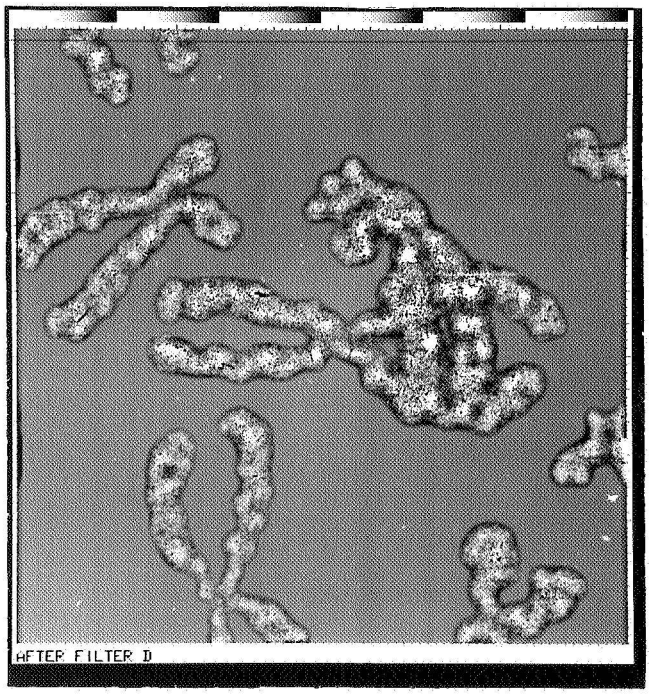
AFTER FILTER D

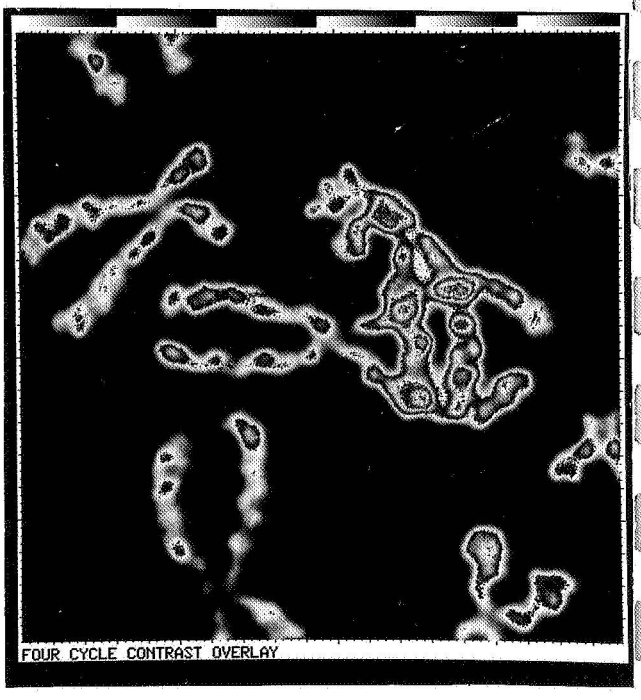
FOUR CYCLE CONTRAST OVERLAY

transducer inserted directly into the ventricle. An example of one frame from such a film is shown in Figure 47. This film was provided by Dr. Russell H. Morgan, Chief of the Radiology Department of John Hopkins University Medical School. Motion picture films have also been received from Dr. Henry D. McIntosh, Head of the Cardiovascular Department of Duke University Medical Center.

Calculation of this sort for a single patient require about three weeks when done by hand. It does seem possible that this measurement and calculation could be accomplished with a computer. The most serious obstacle at the current time is the difficulty of handling the large number of frames (typically 350 frames for one patient) with the film scanning equipment currently available. However, the feasibility of using computer methods could certainly be established by working on a few frames.

SPECTRAL ANALYSIS APPLIED TO BONE X-RAY FILMS

When bone X-rays are inspected closely they reveal a somewhat cobweb-like network called the trabecular network or pattern. An example is shown in Figures 48 and 49. Certain bone diseases will cause this pattern to change. For example, diseases causing calcium loss (osteoporasis) will cause the pattern to become coarser because the finer trabeculae will dissolve. This is a common disease of old age and one sometimes caused by inactivity (as was the case with some of the early astronauts, who lost up to 30% of the calcium in certain bones in a few days in orbit). Also, certain type of bone cancer cause abnormal cell growth which causes abnormal trabecular pattern.

In the case of osteoporasis, the calcium loss is very difficult to measure quantitatively by the usual bone density measurements. The reason

Figure 47

One frame from a high-speed X-ray motion picture of the heart. A radio-opaque dye is injected through a catheter inserted directly into the heart. As the dye and blood mix, the ventricle outline appears and heart size can be measured.

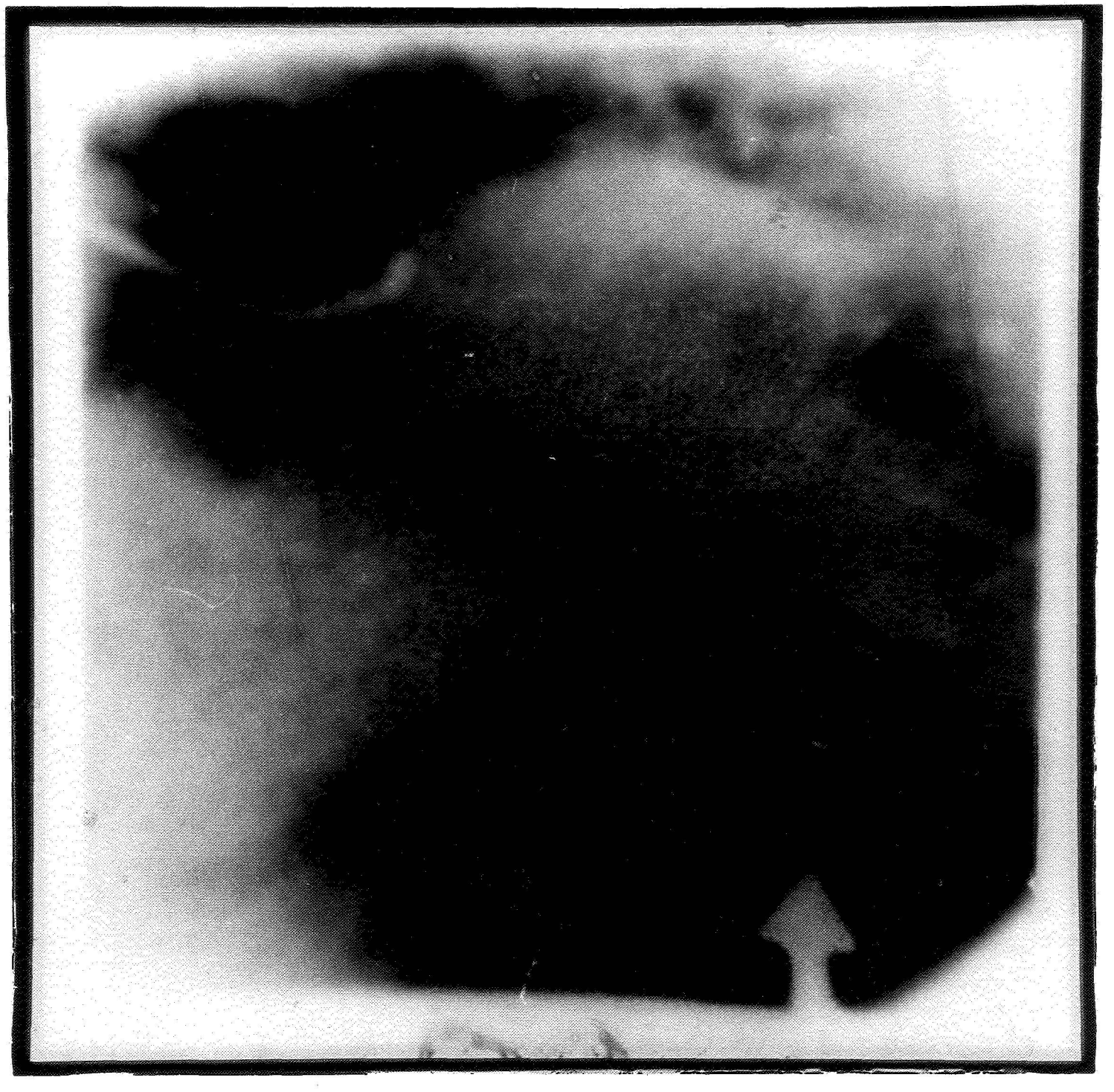

Figure 48

X-ray film of the knee of an eight year old girl suffering from rickets. Substantial calcium has been lost causing the trabecular (bony) pattern to become coarse.

Figure 49

Enlargement of a center portion of Figure 48.

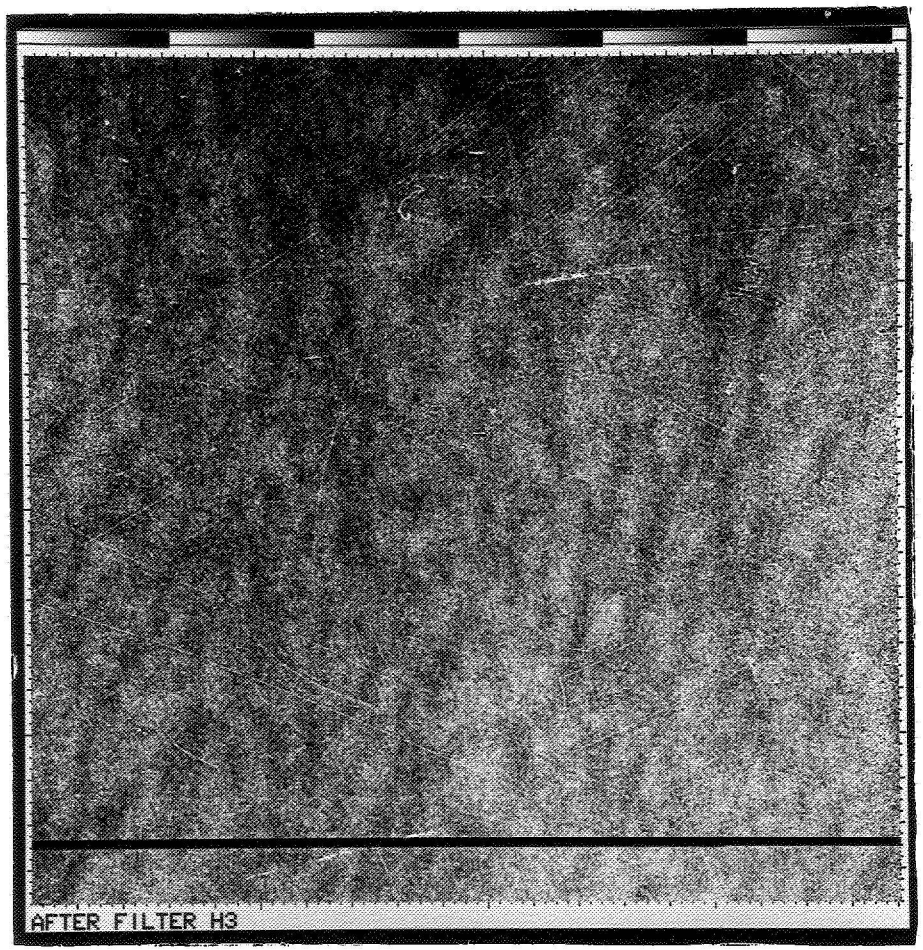
AFTER FILTER H3

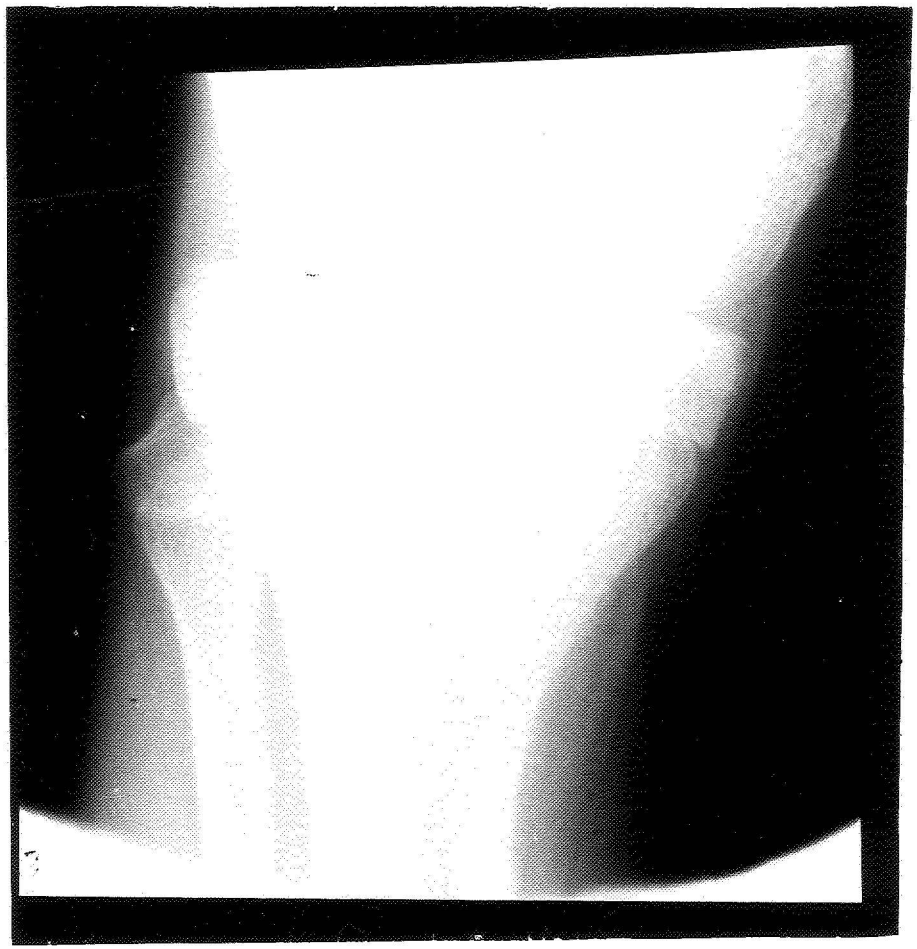

for this is that the density changes are very slight until enormous amounts of calcium are gone and normal background density differences from film to film are very large because of normal variations in exposure and film development conditions.

Therefore, the possibility of detecting loss by looking at pattern change rather than density change is very intriguing. The way to detect the pattern change is to apply a two-dimensional spectral analysis to the X-ray film.

A program has already been written to calculate a one-dimensional spectrum. This simpler case can be used to qualitatively verify the basic assumption that the calcium loss will produce a detectable shift in the frequency spectrum. Figure 50 shows a typical spectrum calculated by this program from the knee picture of Figure 49. The next step contemplated is to apply to analysis to numerous normal and diseased bone X-ray films in order to determine the effect of disease on the "normal" spectrum.

MICROCIRCULATION

The investigation of physiological mechanisms of the blood vascular system requires extensive data acquired at the microscopic level. One technological problem in the field of microcirculation previously not solved, is the capability of on-line quantitative measurement of in vivo preparations. The major problem areas of current interest are: what are the dynamic velocities of the blood in small blood vessels, capillaries, arterioles, venules; what are the changes in geometry of these vessels corresponding to blood flow and, what are the rates of substances entering and leaving these vessels during circulation?

The established method of investigation employs cinematographic techniques of one kind or another. An animal is mounted on a microscope

Figure 50

Typical power spectral density plot obtained by applying a one-dimensional spectral analysis to a single line of Figure 49.

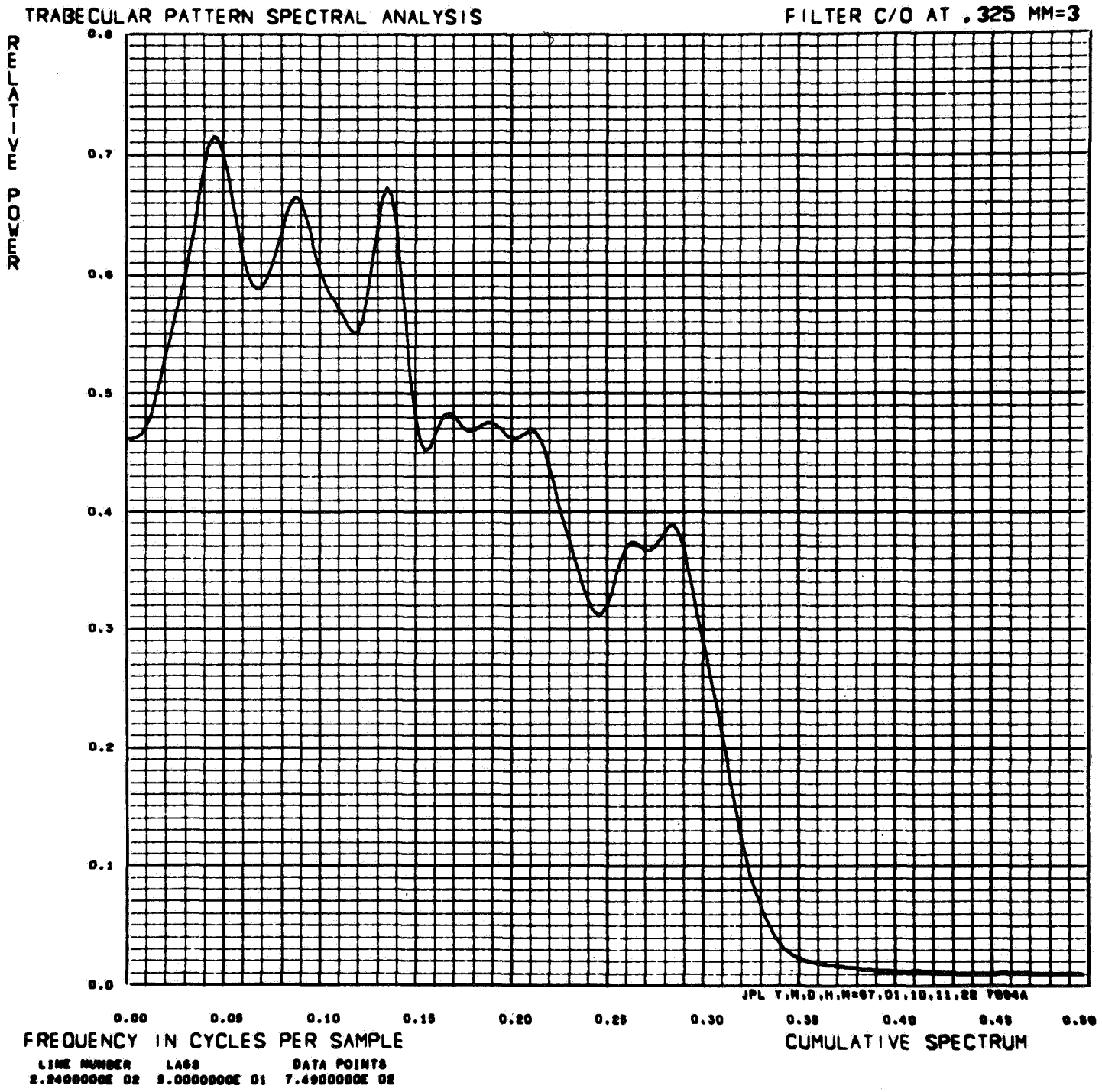
TRABECULAR PATTERN SPECTRAL ANALYSIS
FILTER C/O AT .325 MM=3
RELATIVE POWER
0.8
0.7
0.6
0.5
0.4
0.3
0.2
0.1
0.0
JPL Y,N,D,N,N=67,01,10,11,22 7804A
0.00
0.05
0.10
0.15
0.20
0.25
0.30
0.35
0.40
0.45
0.50
FREQUENCY IN CYCLES PER SAMPLE
CUMULATIVE SPECTRUM
LINE NUMBER
2.24000000E 02
LAGS
9.00000000E 01
DATA POINTS
7.49000000E 02

stage so that certain tissues can be photographed with a motion picture camera. The films are subsequently analyzed by making frame by frame measurements. This is an exceedingly laborious technique requiring hours for a single analysis. In the case of rapid blood flow, where high speed cinematography is required and high light intensity must be used for sufficient illumination, this technique is marginal. Focus becomes a problem and the tissue responds unfavorably to the heat from the light. This technique requires elaborate equipment and highly trained technical assistance for performing the data analysis. However, the chief limitation is the inability of the experimenter to use the data while performing the experiments.

An in vivo experiment may last only a few hours. Each experiment is a different set-up, and any one variable e.g., electrical stimulation, introduction of drugs, etc., must be tested slowly step by step, and on numerous animals since the results of each experiment are not determined until long after it was performed. There is a real need for on-line simultaneous quantitative measurement during the functioning of the preparation.

The detection and measurement of motion (blood flow in this case) shares certain commonality with problems currently being investigated in the bioscience program at JPL. The blood flow is one-dimension simplification of motion detection. It appears reasonable to solve the problem of multi-direction movement by first developing a tool for careful measurement of unidirection motion. At the same time this has produced a valuable contribution to an important related field.

One method for making this measurement might be to use the timing of a television scanning system which might be obtained from a television microscope set up of the in vivo preparation. This technique takes advantage of the intrinsic synchrony of a scanning system as a timing device when superimposed upon the biological events. Our earlier attempts with this technique indicated a promising method, however, the background "noise" of the television system used masked the signal that was sought. Subsequent to our attempt another Laboratory (Dr. Kurt Wiederhelm, University of Washington) is investigating this method.

An alternative technique is to follow the particular biological events with a device used for measuring velocity. An appropriate instrument is the image dissector. This can be used to optically follow an object across a field of view, and with proper calibration will measure continuously the rate of motion. The leading edge of the object is focused in an aperture which creates a photoelectric image. A deflection coil with suitable feedback is able to hold the photoelectric image within the aperture which the object is moving across the field of view. The voltage of the coil is a function of the rate of motion of the object.

A commercial instrument of this kind was focused to monitor a projected image of a microscopic field. In these experiments a frog rana pipiens, was used for the preparation. The web of the hind leg was suitably illuminated and magnified so that a small arteriole was focused across the field. By appropriate optics this was projected onto a ground glass. The image dissector was arranged to scan parallel to the course of blood flow. The voltage output of the coil of the image dissector was continuously monitored with a scanning oscilloscope (Fig. 51).

Figure 51

Experimental preparation for microscopic examination and measurement of vascular bed of frog's hind leg. The image dissector is used to measure rate of blood flow through capillary scanned along 200 microns of its length.

Figure 52

Data showing result from oscilloscope and calculation in determining actual rate of bloodflow. Optical magnification and calibration are used in this calculation.

BIOSCIENCE EXPERIMENT DEVELOPMENT

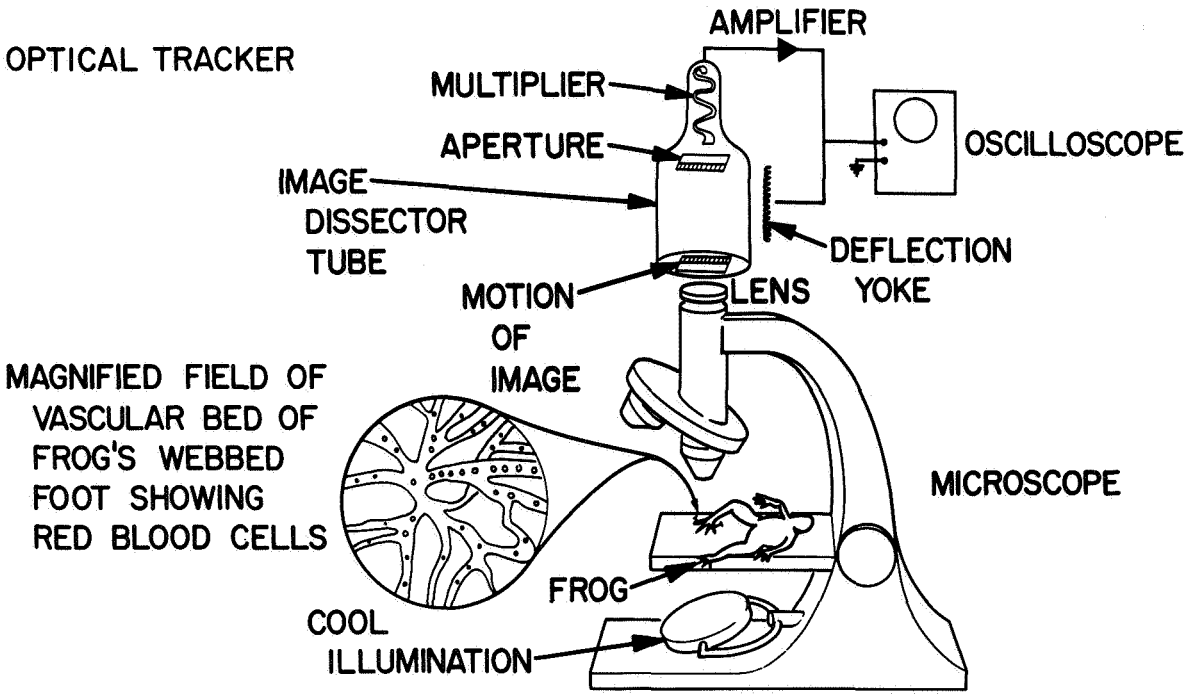

OPTICAL TRACKER MICROSCOPE FOR MEASURING MICROCIRCULATION

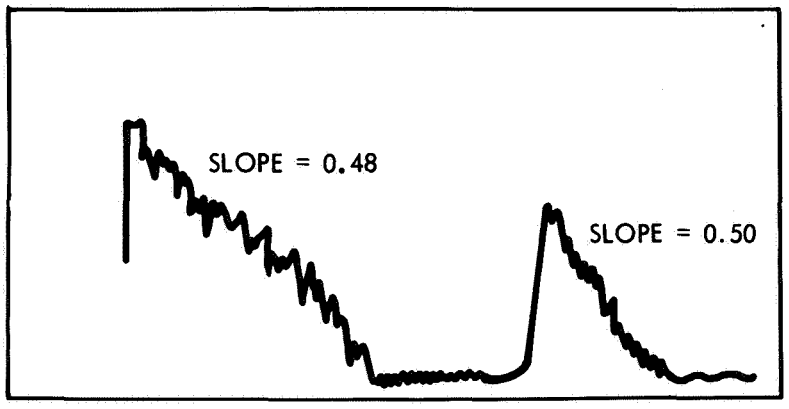

SWEEP = 50 msec/cm
VERTICAL = 100 mv/cm
CALIBRATION = 1.28 cm/v
OPTICAL MAG. 150 x

DATA:

VERTICAL 3.5 cm = 350 mv
1.28 cm/v x 0.35 v = 0.448 cm
0.448 cm x 250 msec = 15.24 mm/sec

VELOCITY 15.24 cm/sec/150x = 101.6 μ/sec

VELOCITY BLOOD FLOW FROG

The results produced on the oscilloscope (Fig. 52) were a "ramp" produced by building up of the coil voltage while the leading edge of a blood cell was in motion. When the cell has passed the field of view, the voltage dropped and the image dissector would catch the edge of another blood cell that had passed through the field (where time is moving from right to left). The slope of the "ramp" is a function of the velocity of blood flow. Calculations are shown.

In one case the blood was moving slowly enough to permit checking this technique with a more direct method. The field of view was calibrated for distance and using a stop watch, the average velocity was measured. Both measurements were in complete agreement.

This new technique should offer a new tool for on-line physiological measurement of blood flow. The same technique might be used to accurately measure changes in the geometric dimensions of the blood vessels. It is believed that this application, or the development of television as a measuring device, could rapidly generate the information necessary to understand the physiology of circulation at the cellular level.

ELECTRON MICROSCOPE RESOLUTION

Because of their limited effective lens aperture and instability, electron microscopes can at best resolve objects down to 5-8 Å. Figure 53 is a picture of an AEI microscope installed at JPL. Figure 54 illustrates the kind of image that can be seen by this kind of instrument (though it is not our picture) in its present state. The molecules of the adenovirus are about 50 Å in diameter and are visible by contrast against a background of phosphotungstic acid. If resolution can be improved to 1 Å, then detailed atomic structure becomes visible. X-ray diffraction methods do resolve 1 Å distances on simple molecules, but only in rare instances for moderately complex substances do these techniques work.

X-ray and electron diffraction methods of atomic structure determination use for diverging diffraction pattern which arises from the crystal under examination when illuminated by an incoming beam. (See Figure 55.) Figure 56b shows the diffraction pattern which is recorded on film when light is passed through the pattern shown in Figure 56a. Because of the divergence there can be no interaction between the various parts of the diffraction pattern. When this pattern is intercepted by a photographic film, all that is recorded is the intensity of the diffraction pattern, while the phases of the pattern's maxima are completely lost. But a knowledge of these phases along with the intensity of the maxima can be used by a computer to prepare a Fourier synthesis of the electron density in the crystal for the purpose of finding the atomic arrangement in the crystal.

Figure 53

AEI Electron Microscope Model EM6

This instrument has the unique ability to tilt its incoming beam under electronic control.

Figure 54

A "good" picture of a crystalline adeno-virus

Molecules are about 50 Å apart. Contrast is obtained by means of negative staining with phosphotungstic acid.

ELECTRON MICROSCOPE

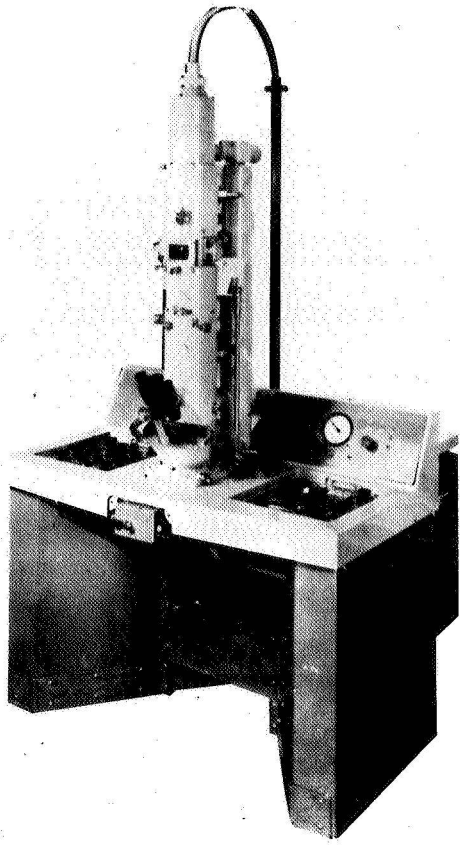

Figure 55

A plane wave "illuminating" a periodic structure from below gives rise to interference combinations called 0th, 1st, 2nd, etc. orders each of which then travels as a wave front moving perpendicular to new wave crest.

Figure 56

Two dimensional

a. pattern

b. associated diffraction pattern

Figure 57

Comparison of small aperture lens, both on and off optical axis and large aperture lens on axis in system illuminated by monochromatic parallel light.

ELECTRON MICROSCOPE FACILITY

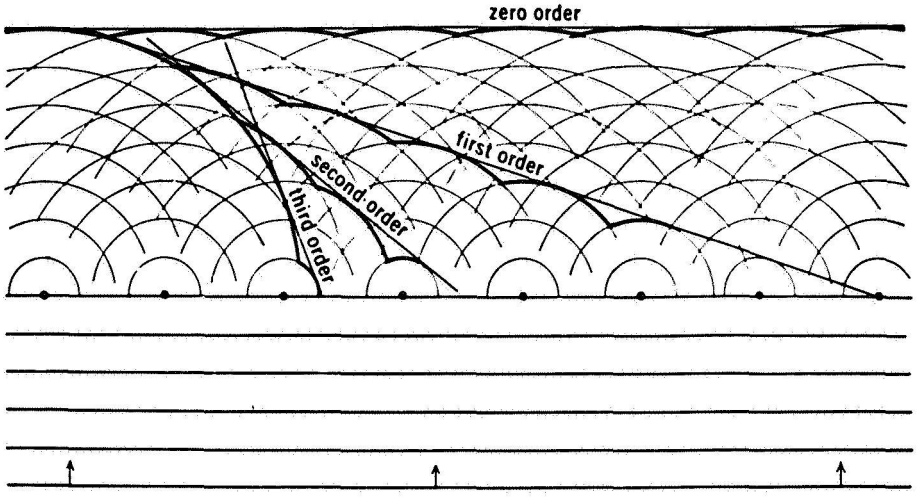

DIFFRACTION ORDERS (MAXIMA) EMERGING FROM APERTURES IN A PERIODIC STRUCTURE

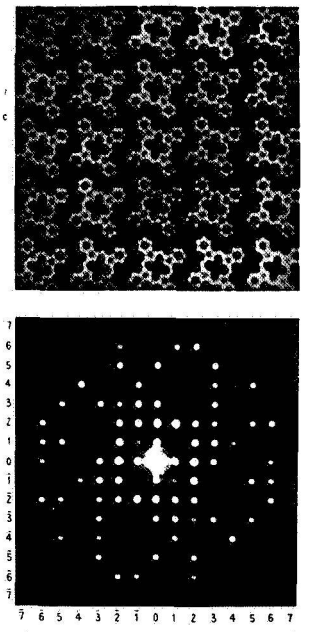

ABOVE: PHTHALOCYANINE MOLECULES
BELOW: DIFFRACTION PATTERN

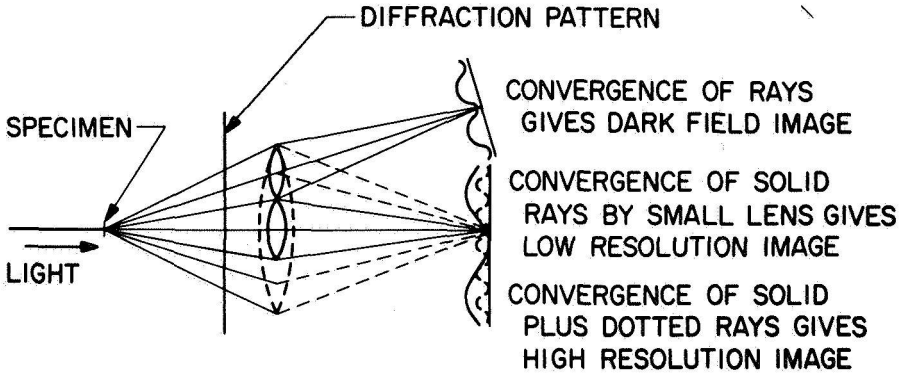

In the case of electron diffraction, if an electron lens is placed between the crystal and the photographic film, the lens can be made to cause those diffraction maxima passing through the lens aperture to converge and interfere in a calculable manner depending upon their relative phases. If the electron lens had an effective aperture of about ten times its present capability, then resolutions of 1 Å would be possible. But there appears to be a theoretical limit equivalent to spherical aberration which stops the lens from being used to collect more diffraction maxima. If the crystal and incident beam are tilted relative to the lens, or if the lens aperture in the rear focal plane of the objective lens is shifted, then different diffraction maxima can be made to interfere in a way that reveals their relative phases. (See Figure 57.)

Simulation of this method has been performed at visible wave lengths on larger targets on an optical bench. Figure 58b shows a high resolution image whose repeat unit is indicated by the square. The diffraction pattern of this image is shown in Figure 58a. Suppose now a poor lens (one with a limited aperture) were used and allowed only those diffraction maxima indicated in Figure 58c to pass through its opening. Because the higher frequency components were not included, the resultant image in Figure 58d has lost its sharpness and some of the image details are missing. Figure 58e shows some of the off-axis diffraction maxima which can be made to go through the restricted lens upon shifting the lens to one side of the optical axis. An image is formed in Figure 58f which no longer resembles the original object but which can be analyzed to produce phase information on the higher order diffraction maxima which produced it.

Figure 58

Optical Bench Simulation of Problem

a. Large aperture gives full diffraction pattern

b. High resolution possible if able to use large aperture, does not exist for electron microscope.

c. Restricted aperture allowing only central diffraction maxima to pass.

d. Low resolution image resulting from figure 58c.

e. Restricted aperture allowing only off-axis diffraction maxima to pass.

f. Low resolution "dark field" image resulting from Figure 58e. Note the lack of resemblance to image formed in Figure 58d.

Figure 59

Computer Reconstruction From Fourier Analysis of Images in Figures 58d and f.

a. Reconstitution of 1/4 cell repeat unit as seen in Figure 58d (low resolution image)

b. Reconstitution of full unit cell from Fourier components obtained from analysis of Figure 58d. Note loss of image detail.

c. Reconstitution of 1/4 cell taking phase and magnitude of Fourier components from both on-axis (Figure 58d) and off-axis (Figure 58f) images to form single high resolution image resembling Figure 58b.

d. Full unit cell simulation of high resolution (See Figure 59c). Note increased sharpness and appearance of non-round shape.

ELECTRON MICROSCOPE FACILITY

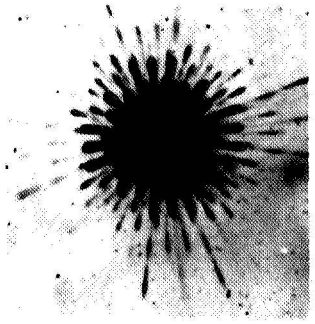
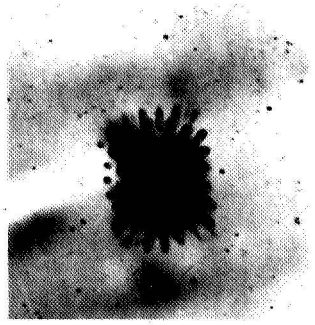
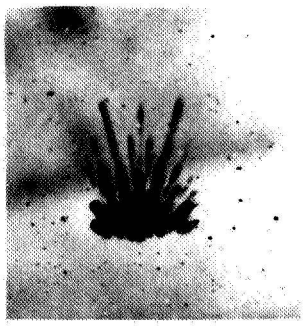

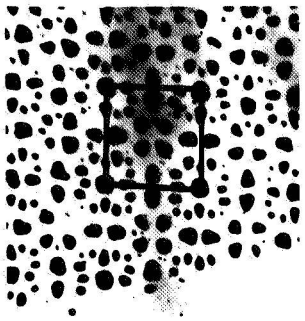
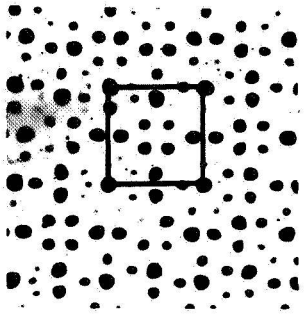
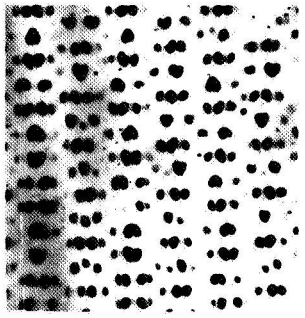

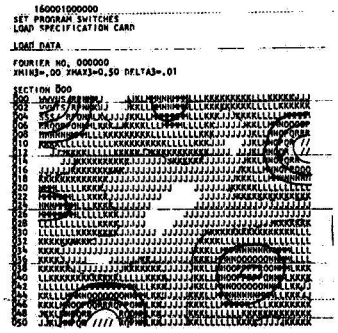

1/4 UNIT CELL-LOW RESOLUTION

1/4 UNIT CELL-SIMULATION OF HIGH RESOLUTION

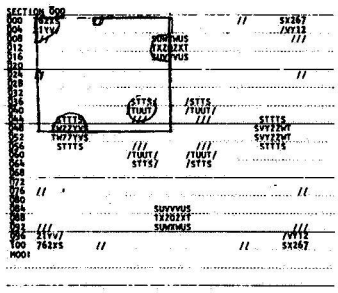

FULL UNIT CELL-LOW RESOLUTION

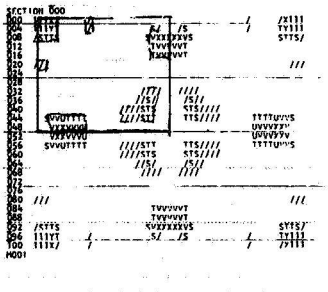

FULL UNIT CELL-SIMULATION OF HIGH RESOLUTION

COMPUTER RECONSTRUCTION FROM FOURIER TRANSFOM OF DIFFRACTION MAXIMA

A Fourier analysis can also be performed on the central-axis image Figure 58d. A reconstitution of the low resolution image from its Fourier components is shown in Figure 59 a and b. If to the Fourier components for the low resolution image are added the Fourier components from the off-axis diffraction maxima (from Figure 58e), the computer synthesizes a high resolution image in Figure 59 c and d resembling the original object Figure 58b. (Note the sharpening of edges as higher frequency components are added.) This kind of computer reconstitution is used in X-ray diffraction and the kind of final product which is to be expected is indicated in Figure 60 which shows the electron density map of a simple compound hexamethylbenzene.

As the instrument stands now, some crystalline organic specimen has been stable enough to give rise to a diffraction pattern shown in Figure 61.

Mathematically, the above method is well understood. What problems are encountered when attempts are made to apply it? The electron beam which is used in the microscope is very energetic, and when it is applied in high concentration onto an organic specimen for examination, the specimen melts from the heat. Also, organic substances which are of interest are low in contrast which has led to the practice of shadowing or immersing the specimen in some heavy metal such as platinum or tungston. Since these methods only give superficial information, something must be done to get images from the original organic materials. The solution may be to install a sensitive television camera directly in the microscope column and place the operation of the microscope under computer control in order to accelerate specimen manipulating during the picture taking sequence. Such modifications have been initiated. It is planned to feed the television image directly (after digitizing) into the computer memory for analysis and subsequent synthesis. Specimen motion (translation, rotation, and tilt) and microscope examination should be completely automated.

Figure 60

Atomic resolution obtained by X-ray methods for simpler substances. This resolution is goal of present effort on electron microscope, but is expected to be applied to more complex organic substances.

Figure 61

Diffraction pattern obtained in our instrument of indanthrene olive crystal.

ELECTRON MICROSCOPE FACILITY

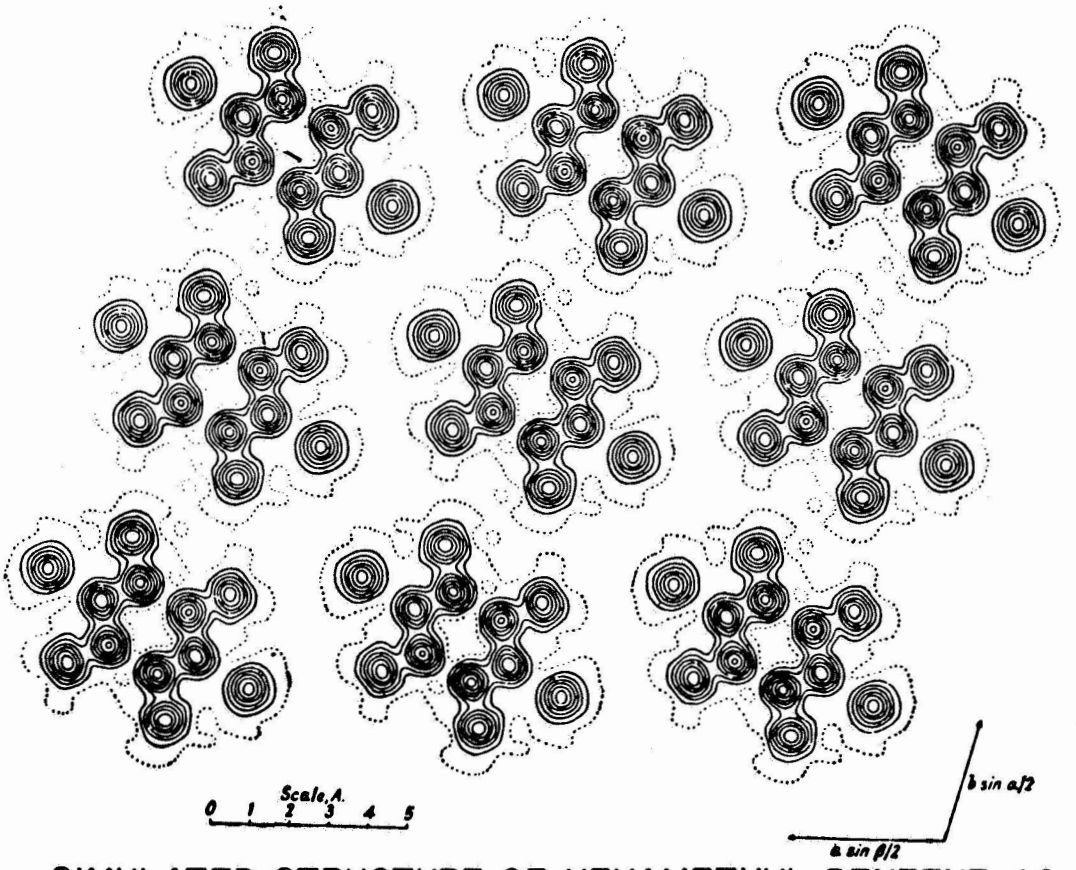

SIMULATED STRUCTURE OF HEXAMETHYL BENZENE AS DETERMINED BY X-RAY CRYSTALLOGRAPHIC METHODS